Sensor fusion for position estimation of artists on stage by coupling data from two UWB/IMU sensors

M. F. Hoekstra

Master of Science Thesis

TU Delft Delft University of Technology

Delft Center for Systems and Control

Sensor fusion for position estimation of artists on stage by coupling data from two UWB/IMU sensors

Master of Science Thesis

For the degree of Master of Science in Systems and Control at Delft University of Technology

M. F. Hoekstra

March 14, 2025

Faculty of Mechanical Engineering (ME) · Delft University of Technology

The work in this thesis was supported by Sendrato. Their cooperation is hereby gratefully acknowledged.

Abstract

The localization and tracking of artists on stage enables theatre spotlights to automatically follow the artist's movements. The company Sendrato utilizes Ultra-Wideband (UWB) systems for this purpose, but the position estimation accuracy decreases when the sensors operate in a Non-Line-of-Sight (NLOS) environment. To prevent the body from blocking the UWB signals, Sendrato places two UWB tags on the hips of the artist and averages the two estimated tag positions. Inertial Measurement Units (IMUs) offer an additional means for location tracking, providing inputs to calculate position, velocity, and orientation estimates independent of the environment, but suffer from accumulative error due to integration drift. This thesis studies how Sendrato can improve position tracking accuracy with UWB data by incorporating IMU sensor data. Additionally, the thesis investigates how the two tags can be coupled to correct for each other's inaccuracies. Hence the thesis studies how the sensor fusion of two coupled UWB/IMU sensors, attached to a person's hips, can be used to improve position tracking accuracy compared to using two separate UWB tags. This gives rise to a research approach consisting of two parts. To investigate the potential of UWB/IMU sensor fusion for position tracking accuracy, an Extended Kalman Filter (EKF) fusing IMU and UWB measurements is implemented and compared to UWB-only position tracking algorithms. Additionally, it is investigated whether IMU bias state estimation, Zero Velocity Update (ZUPT) implementation and NLOS detection and mitigation can further improve the UWB/IMU EKF tracking accuracy. The second part researches the potential of coupling two UWB/IMU tags for position tracking accuracy. Previous methods inspired to use knowledge of the fixed relative distance between the tags to correct position estimates from each tag. This research developed this approach by including an equality constraint on the distance between the tags into the EKF. An experiment is conducted where the joint UWB/IMU EKF is tested on a known walked trajectory containing several stationary points. The results show that the tightly coupled UWB/IMU EKF can help smooth faulty UWB measurements, correct stationary points with a ZUPT, and identify IMU bias. Moreover, enforcing a fixed distance between joint tags allows for mutual correction of their trajectories, though the impact on the averaged trajectory may be less significant. All of these techniques show potential for improving position tracking accuracy compared to a loosely coupled UWB-only algorithm. However, the methods all showed limitations, presumably caused by the data quality. An important

direction for future work would be to continue this research with better calibrated UWB data.

Table of Contents

List of Figures

Preface

This document contains my Master of Science graduation thesis for the master Systems and Control. The idea for this thesis topic started with the ambition to gain experience in an engineering company before graduating. When discussing the idea of doing the thesis project at a company, my supervisor Manon Kok informed me of Sendrato, a company that develops technologies for artists on stage. Given my interest in motion capture applications, in combination with my experience with and enthusiasm for dance performances, I was immediately drawn to this topic and I was highly motivated to be able to contribute to the development of this technology.

I would like to thank my supervisor dr. Manon Kok for her invaluable assistance and feedback while conducting the research and writing this report. I also appreciate her enthusiastic character during our biweekly meetings, and her compassion during difficult personal circumstances. Additionally, I would like to thank Dr. René Laterveer for suggesting the research topic and Dr. Arjen Schoneveld and Daan Schoneveld for their insights into the technical aspects of the sensor system and for helping me obtain the necessary data for my research. Finally, I want to thank my loved ones for their support throughout this master's thesis project.

Delft, University of Technology — M. F. Hoekstra
March 14, 2025

Chapter 1

Introduction

1-1 Background and motivation

Localization and tracking have been extensively researched over the past few decades. In recent years, the rapid development of wireless communication technology in smartphones and wearables has enabled many applications for user localization and tracking. Various sectors, including healthcare, industry, surveillance, and more, have been utilizing these applications and services [2]. Some examples of localization and tracking include optimizing traffic flow, monitoring Alzheimer's patients, and smart homes [3], [4], [5]. In general, localization refers to determining the position coordinates of a sensor, while tracking refers to the continuous localization over time, where the position and velocity are estimated at each time instant [6], [7]. This research is in the context of another sector, which is the theatre industry. High-accuracy tracking of artists on stage enables the spotlights to automatically follow the artist's movement on the stage. The benefit of automating the spotlights is that a large number of artists on stage can easily be followed by their own individual spotlight. Additionally, artists no longer have to worry about missing their cue for the lighting. During theatre performances, it needs to be ensured that the tracking of the artists happens in real-time and flawlessly, as localization mistakes cannot be filtered out after the event and are immediately noticed by the audience. The thesis is executed in collaboration with Sendrato. The research focuses on their product TraXYZ, a technology that tracks the position of artists on stage to automatically operate light, sound, video, and more.

In general, position tracking relies on signals and systems such as GPS, visual cameras, inertial navigation sensors, and LiDAR [8]. To track artists on stage, Sendrato makes use of an Ultra-Wideband (UWB) system and Inertial Measurement Units (IMUs). UWB is a low-power consumption radio technology that utilizes signal pulses with a duration of one nanosecond [9], [10], [11]. These short pulses enable the distinction between multiple propagation paths and filtering them out accordingly [10]. These characteristics make UWB systems suitable for position estimation for localization and tracking. Nevertheless, UWB systems are still affected by multipath or Non-Line-of-Sight (NLOS) conditions [9]. NLOS refers to the prolongation

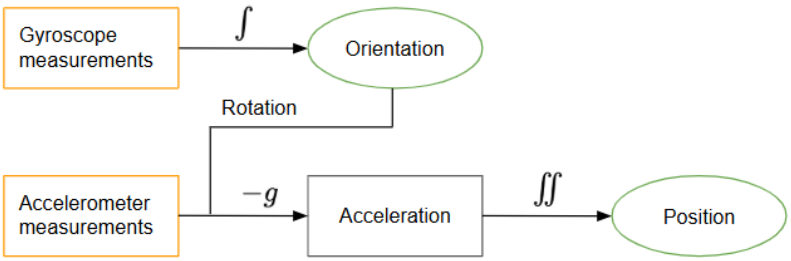

Figure 1-1: The process of 'dead-reckoning' for estimating position and orientation (pose) based on accelerometer and gyroscope measurements.

of signal flight time due to obstacles in the environment that block the signals, resulting in inaccurate position estimates [9], [12]. The additional sensor system used by Sendrato, the IMU sensor, includes a 3D accelerometer and a 3D gyroscope. The accelerometer measures the acceleration by measuring the external specific force acting on the sensor. The gyroscope measures the angular velocity, which gives information about orientation. From the gyroscope and accelerometer measurements, the position and orientation can be derived by means of 'dead-reckoning'. This process is illustrated in Figure 1-1. As can be seen in the figure, the measurements obtained can be integrated to result in 6D position and orientation (pose) estimation. However, when the measurements contain bias and noise, the errors grow over time because of this integration process. This is called 'integration drift' [13].

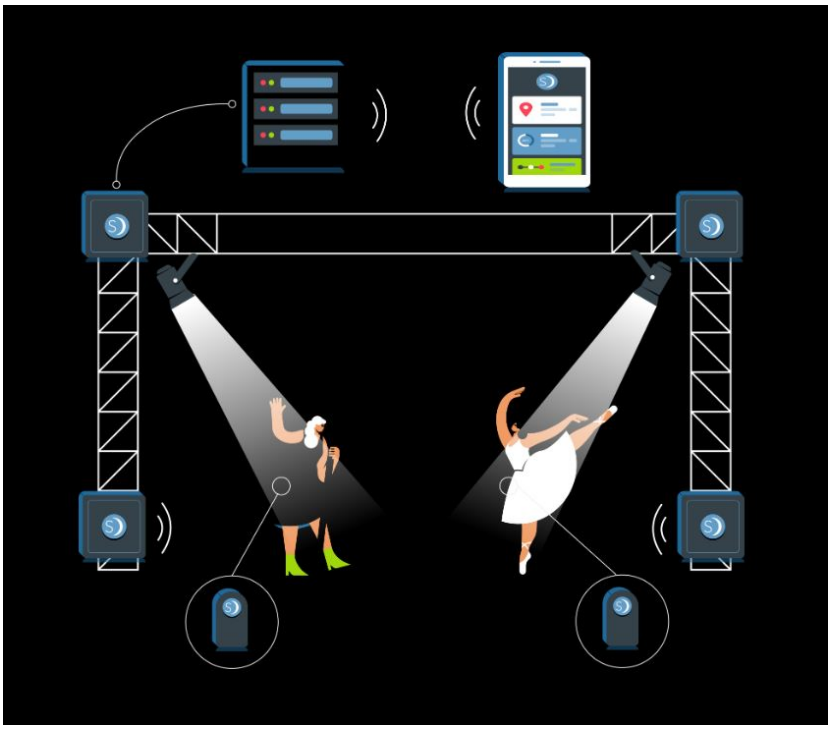

Figure 1-2: Illustration of the TraXYZ setup with anchors around the stage and tags carried by the artists [1].

The TraXYZ setup of Sendrato consists of anchors and tags (Fig. 1-2 and 1-3). Anchors (also referred to as receivers, sources, or beacons in literature) are stationary nodes that send and receive signals to and from the tags. Tags are the mobile sensors carried by the artists of which the location needs to be tracked. The location of the anchors can be calculated beforehand and is therefore known, while that of tags needs to be determined during tracking. Each tag is equipped with a UWB sensor and an IMU sensor. The UWB sensor provides Two Way Ranging (TWR) data. Estimating the distance between anchor and tag is called ranging. During two-way ranging, the anchor and tag exchange multiple signals, so their clocks do not need to be fully synchronized beforehand [14]. The UWB sensors of Sendrato directly provide a distance in meters. This distance represents the shortest signal path between anchor and tag when NLOS conditions are absent. The accelerometer and gyroscope contained in the IMU sensor provide data for acceleration and angular velocity, respectively. This happens independently of the anchors. The IMU sensor also contains a magnetometer, but this will not be used due to magnetic disturbances in theatre environments. Therefore, this report will not discuss the magnetometer any further.

(a) Tags **(b)** Anchor

Figure 1-3: TraXYZ tags and anchor [1].

A disadvantage that comes with tracking a person using a UWB system is that the radio signals can be blocked by the user's body, causing NLOS problems. This is because the human body contains a high percentage of water, which can cause delays in the UWB signals. Therefore, the best placement for a single UWB sensor would be the top of the head [15]. However, this is not always practical, especially in theatre performances where the tag needs to be invisible to the audience. Sendrato's solution to this, while still addressing NLOS issues, is to attach two sensors on opposite sides of the user's body and combine their data to estimate position. For that reason, Sendrato chooses to place two tags on the hips of the artist.

Currently, TraXYZ relies primarily on UWB-based tracking, despite the availability of IMU measurements. Regarding the two tags attached to the user's hips, both tags are processed separately to result in two position estimates. Thereafter, the centroid of the two tag positions is taken as the final position estimate of the artist. However, this can lead to less accurate tracking if one or more tags give erroneous or no data. This thesis project studies how the (UWB-only) position tracking accuracy of TraXYZ can be improved, by researching how all

available data from the UWB sensor, the IMU sensor, and the two tags can be combined and utilized for accurate localization and tracking of the artists.

The aim of this research essentially comes down to researching 'sensor fusion'. Sensor fusion can be defined as: "*The combining of sensory data or data derived from sensory data from disparate sources such that the resulting information is in some sense better than would be possible when these sources were used individually [16].*" Hence, for this thesis the sensor fusion of UWB with IMU, and two UWB/IMU sensors placed on the hips, needs to be researched.

The goal of Sendrato leads to the main question for this research:

"How can the sensor fusion of two coupled UWB/IMU sensors, attached to a person's hips, be used to improve position tracking accuracy compared to using two separate UWB tags?"

To answer this question, the research aims to delve into the following subquestions:

1. What potential does UWB/IMU fusion have for position tracking accuracy?
2. What potential does fusing the two tags have for position tracking accuracy?

By addressing these subquestions, this research aims to provide an analysis of the contribution of IMU data and joint tags to the UWB-only tracking system of TraXYZ.

1-2 Organization

Chapter 2 of this report provides an overview of the technical background concerning UWB and IMU sensors and related work on the research topic. It starts with an explanation of the modelling of the UWB and IMU measurements provided by TraXYZ. Subsequently, techniques to perform position estimation with only UWB data are described. This is used as a baseline that needs to be improved. The chapter continues with a description of related work and the state of the art in sensor fusion of multiple UWB/IMU sensors attached to a human body for location tracking.

Thereafter, Chapter 3 presents the algorithm developed in this research for the UWB/IMU sensor fusion and the sensor fusion of two UWB/IMU tags. All sections provide a detailed explanation of a component of this algorithm. That is, the filtering algorithm for UWB/IMU sensor fusion, IMU bias estimation, Zero Velocity Update (ZUPT) implementation, NLOS detection and mitigation, and the sensor fusion method for two tags. The final algorithm with all components is given in Section 3-3.

Chapter 4 starts with a description of the experiments executed to acquire data for testing the algorithm, where the actual walking trajectory is known. The effects and potential of the

method's components applied to the acquired dataset are analyzed in the next sections. This includes the effects of incorporating the IMU data and of joining the two tags, for different cases such as the addition of bias estimation and a Zero Velocity Update.

Finally, the conclusion in Chapter 5 provides answers to the research questions defined in the previous section. It reflects on the findings in Chapter 4 and discusses the insights on the improvement of the tracking accuracy of Sendrato's TraXYZ.

Chapter 2

Related work

This chapter is dedicated to related work on the sensor fusion of UWB and IMU data and the sensor fusion of two UWB/IMU tags attached to the person. It begins with an explanation of the modelling of UWB and IMU measurements. The following section delves into current methods for position estimation using only UWB measurements. Currently, TraXYZ processes the measured distances between anchors and tags using an Extended Kalman Filter (EKF) or an Extended Finite Impulse Response (EFIR) filter combined with a NLOS detection and mitigation method, without including IMU measurements. This is explained in Section 2-2. Thereafter, algorithms for UWB/IMU sensor fusion found in literature are discussed, as well as previous research on the fusion of two tags attached to a person.

In general, there are two ways of performing sensor fusion: loosely coupled and tightly coupled. In the case of a loosely coupled approach, measurements from each individual sensor are first processed. Subsequently, these preprocessed measurements are combined to determine the final outcome. Conversely, a tightly coupled approach involves using the 'raw' measurements from all sensors directly to calculate the final result [17]. A tightly coupled system thus directly incorporates the distance measurements provided by the UWB system in the algorithm, rather than preprocessing this data to result in preliminary positions. There exist UWB/IMU sensor fusion methods based on a loosely coupled algorithm, for example [18] and [19]. Although a loosely coupled approach might in some cases be more practical, some information can get lost during the preprocessing of the measurements. This can happen because of the statistical distribution used to approximate the data [9]. In a tightly coupled approach, all available data is included to compute the final outcome, and outlier rejection opportunities are often included. For those reasons, some literature claims that a tightly coupled system performs better in terms of accuracy and robustness [17], [20]. Currently, Sendrato processes the two tags separately to result in two position estimates and ultimately outputs the averaged position. This is considered a loosely coupled approach. The goal of this thesis is to fuse all available sensor data from both tags directly in one algorithm and investigate the effects. Therefore, this report mainly describes tightly coupled approaches for sensor fusion of two tags.

2-1 Modelling of sensor measurements

To develop algorithms for UWB/IMU sensor fusion, the data of both sensor types need to be modelled. When the UWB data contains outliers, these can be incorporated into the measurement model [9] or the data can be preprocessed to mitigate the outliers before inserting it into the fusion algorithm [12]. Both the modelling of the sensor data and the handling of UWB outliers are discussed in this section.

2-1-1 Modelling of UWB measurements

TraXYZ utilizes a UWB system that provides Two Way Ranging (TWR) measurements. During two-way ranging, the anchor and tag exchange multiple signals, so their clocks do not need to be fully synchronized beforehand [14]. Some literature that uses TWR-type UWB data describes the data as the measured Time of Flight (ToF) of a signal's round trip. This has to be multiplied by the propagation speed of the signal to obtain the distance between the anchor and the tag [12]. However, the UWB sensors investigated for this project directly provide a distance in meters. This distance represents the shortest signal path between anchor and tag. In case of NLOS conditions, the measured distance contains positive bias [14].

The measured distance $y^i_{d,t}$ between the tag and anchor i can be modeled as [21], [22]:

$$y^i_{d,t} = d^i_{\text{true},t} + e^i_{d,t} = \|p^i_{\text{anc}} - p_{\text{tag},t}\|_2 + e^i_{d,t}, \tag{2-1}$$

where p^i_{anc} is the position of the i-th anchor, $p_{\text{tag},t}$ is the position of the UWB tag, and $e^i_{d,t}$ is the Gaussian error term. The positions of the stationary anchors p^i_{anc} can be calculated beforehand and are therefore assumed to be known. The UWB setup is calibrated with calibration software of Sendrato. The anchor positions are calibrated to the local geographic coordinate system in which the person is localized, defined as the navigation frame. Hence this thesis assumes that the UWB coordinate frame is aligned with the Earth's coordinate frame. The position of the tag $p_{\text{tag},t}$ used in the UWB model of Eq. (2-1) is therefore defined in this navigation frame.

Existing literature discusses managing UWB outliers before inserting them into a position estimation algorithm. For example, the UWB measurements can be preprocessed using a Kalman Filter (KF) [12] or Non-Linear Least Squares (NLS). These approaches filter out the main outliers of the UWB data before inserting them into a fusion algorithm. However, for this thesis, a tightly coupled fusion algorithm is researched, where the goal is that the IMU data corrects for erroneous UWB data. Therefore, for this research, it is chosen to not delve further into using a different algorithm to filter out UWB outliers beforehand. Alternatively, the work presented in [9] offers an alternative model for the UWB measurements. The article states that the heavy-tailed asymmetric distribution can model the UWB data while incorporating the outliers, rather than the normal distribution of Eq. (2-1). However, when bayesian filtering techniques are used, the measurements are assumed to be Gaussian.

2-1-2 Modeling of IMU measurements

Inertial Measurement Units (IMUs) can be used for pose estimation, where the object's pose is formed by its position and orientation. The IMU consists of a 3-axis accelerometer and a 3-axis gyroscope. The accelerometer measures external specific force acting on the sensor and the gyroscope measures angular velocity (rate of change of the sensor's orientation) [13]. After modeling the accelerometer and gyroscope measurements, the measurement models are used as inputs to a dynamic model.

To understand the models of the accelerometer and gyroscope measurements, some coordinate frames need to be introduced first. Primarily used for these models are the body frame b and the navigation frame n [13].

- **Body frame (b-frame):** The coordinate frame of the IMU sensor itself, with the origin located in the center of the IMU and the axes aligned to its casing. All IMU measurements are resolved in the b-frame.
- **Navigation frame (n-frame):** The local geographic coordinate frame in which the object is localized. If the sensor travels large distances, it can be necessary to move the n-frame along the surface of the earth. Since this is not the case in the context of theatres, the n-frame is considered stationary throughout this report.

Hence, the goal of pose estimation is to determine the position and orientation of the b-frame with respect to the n-frame. Let $\omega^b_{nb,t}$ denote the angular velocity of the body frame b with respect to the navigation frame n, then the gyroscope measurements $y_{\omega,t}$ can be modeled by [13]

$$y_{\omega,t} = \omega^b_{nb,t} + \delta^b_{\omega,t} + e^b_{\omega,t}. \tag{2-2}$$

In this model $\delta^b_{\omega,t}$ denotes the gyroscope bias and $e^b_{\omega,t} \sim \mathcal{N}(0, \Sigma_\omega)$ describes the Gaussian noise. Here it is assumed that $\Sigma_\omega = \sigma^2_\omega I_3$ with I_3 the 3×3 identity matrix. The bias $\delta^b_{\omega,t}$ can be considered constant or slowly time-varying.

The external specific force f^b_t measured by the accelerometer consists of the linear acceleration a^n_t and gravity vector g^n. The accelerator measurements $y_{a,t}$ can be modeled by [13]

$$\begin{aligned} y_{a,t} &= f^b_t + \delta^b_{a,t} + e^b_{a,t} \\ &= R^{bn}_t(a^n_t - g^n) + \delta^b_{a,t} + e^b_{a,t}, \end{aligned} \tag{2-3}$$

with $\delta^b_{a,t}$ the accelerometer bias, $e^b_{a,t} \sim \mathcal{N}(0, \Sigma_a)$ the Gaussian noise and $\Sigma_a = \sigma^2_a I_3$. Furthermore, R^{bn}_t is the rotation matrix representing the rotation from the n-frame to the b-frame at time t. The accelerometer bias can again be treated as constant or slowly time-varying.

The measurements used in the models above are resolved in the b-frame. To compute the position and orientation in the n-frame, the dead-reckoning process illustrated in Figure 1-1 is used [17]. By using Euler discretization with IMU sampling interval Δt, a dynamic model

for position, velocity, and orientation of the IMU can be composed, which uses the IMU measurements $y_{a,t}$ and $y_{\omega,t}$ as inputs [13], [9], [16]:

$$\begin{aligned} p_{t+1}^n &= p_t^n + \Delta t v_t^n + \frac{(\Delta t)^2}{2} a_t^n \\ &= p_t^n + \Delta t v_t^n + \frac{(\Delta t)^2}{2} R_t^{nb}(y_{a,t} - \delta_{a,t}^b - e_{a,t}^b) + \frac{(\Delta t)^2}{2} g^n, \end{aligned} \tag{2-4a}$$

$$\begin{aligned} v_{t+1}^n &= v_t^n + \Delta t a_t^n \\ &= v_t^n + \Delta t R_t^{nb}(y_{a,t} - \delta_{a,t}^b - e_{a,t}^b) + \Delta t g^n, \end{aligned} \tag{2-4b}$$

$$q_{t+1}^{nb} \approx \left(I_{4\times 4} + \frac{\Delta t}{2} S(y_{\omega,t} - \delta_{\omega,t}^b) \right) q_t^{nb} + \frac{\Delta t}{2} \bar{S}(q_t) e_{\omega,t}^b. \tag{2-4c}$$

The gyroscope measurements modelled by Eq. (2-2) are integrated to arrive at orientation q^{nb} of the b-frame with respect to the n-frame. The accelerometer measurements modelled by Eq. (2-3) are rotated to the n-frame after which the gravity g^n is subtracted. This results in the acceleration a^n, which is integrated once to obtain velocity v^n and integrated again to obtain position p^n. The bias and noise contained in the measurements are also integrated in the process, leading to integration drift. Therefore, the computed position and orientation are only accurate on a short time scale [13].

The orientation is described by the unit quaternion q_t^{nb}. The unit quaternion has an advantage over the rotation matrix because it provides a minimal representation of orientation. It also offers a unique representation of orientation after enforcing $q_0 \geq 0$ and avoids the gimbal lock effect, which is a problem with Euler angles [13], [16]. The unit quaternion can be converted to a rotation matrix with the formula [16]

$$R^{nb} = \begin{pmatrix} 2q_0^2 - 1 + 2q_1^2 & 2q_1q_2 - 2q_0q_3 & 2q_1q_3 + 2q_0q_2 \\ 2q_1q_2 + 2q_0q_3 & 2q_0^2 - 1 + 2q_2^2 & 2q_2q_3 - 2q_0q_1 \\ 2q_1q_3 - 2q_0q_2 & 2q_2q_3 + 2q_0q_1 & 2q_0^2 - 1 + 2q_3^2 \end{pmatrix}, \tag{2-5}$$

where q is resolved in the navigation frame (q^{nb}).

The matrices in Eq. (2-4c) are skew-symmetric matrices defined as [16]

$$S(\omega) = \begin{pmatrix} 0 & -\omega_x & -\omega_y & -\omega_z \\ \omega_x & 0 & -\omega_z & \omega_y \\ \omega_y & \omega_z & 0 & -\omega_x \\ \omega_z & -\omega_y & \omega_x & 0 \end{pmatrix}, \tag{2-6}$$

$$\bar{S}(q) = \begin{pmatrix} -q_1 & -q_2 & -q_3 \\ q_0 & q_3 & -q_2 \\ -q_3 & q_0 & q_1 \\ q_2 & -q_1 & q_0 \end{pmatrix}. \tag{2-7}$$

As was mentioned in the modelling of the gyroscope and accelerometer, the bias on the measurements can be considered constant or slowly time-varying. In the case of slowly time-varying bias, the bias could be estimated in the state vector along with the position, velocity

and orientation. The bias could then be modeled as a random walk [23]

$$\delta^b_{a,t+1} = \delta^b_{a,t} + e^b_{\delta_a,t}, \tag{2-8a}$$

$$\delta^b_{\omega,t+1} = \delta^b_{\omega,t} + e^b_{\delta_\omega,t}, \tag{2-8b}$$

where the Gaussian noise terms $e^b_{\delta_a,t}$ and $e^b_{\delta_\omega,t}$ determine how constant the bias will be.

2-2 Position estimation

Since the research aims to compare position tracking through UWB/IMU sensor fusion with position tracking without usage of IMU data, methods for position estimation with only UWB data are studied to provide a baseline for the research. Furthermore, methods for position estimation with both UWB and IMU that are most commonly found in literature are summarized in this section.

TraXYZ is known to use an Extended Finite Impulse Response (EFIR) filter, as given in [24], [25], [26], or an Extended Kalman Filter (EKF) to estimate position with UWB data only. The EKF filter will be explained later in this section. The EFIR algorithm is similar to the EKF and is also suitable for nonlinear systems, but eliminates the use of noise covariance matrices and initial values for the state and covariance. The objective of this research is to incorporate the IMU sensor in position tracking. Therefore this thesis will focus on fusion algorithms such as Kalman Filters (KFs).

2-2-1 Position estimation without IMU

One method to estimate position based on UWB distance measurements is 'multilateration' [14], [27]. Let $y^i_{d,t}$ be the measured UWB distance as defined in Eq. (2-1). Multilateration assumes that the tag is located somewhere on the circle with radius $y^i_{d,t}$ around the anchor. This means that the tag is localized at the intersection point of all circles around the anchors [14]. Multilateration comes down to solving a system of equations as shown in [27]. However, this technique requires data from at least three anchors [20]. Furthermore, the system of equations can have multiple solutions or no solution at all due to NLOS errors. Therefore, the localization problem is commonly formulated as a Non-Linear Least Squares (NLS) problem, which is then solved with, for example, Gauss-Newton [14]. The NLS problem is formulated as [28]

$$\hat{p}_{\text{tag},t} = \arg\min_{p_{\text{tag},t}} \sum_{i=1}^{\#\text{anc}} (y^i_{d,t} - \|p_{\text{tag},t} - p^i_{\text{anc}}\|)^2. \tag{2-9}$$

Additionally, Bayesian filtering algorithms can be used to estimate position. A widely used state estimator for UWB location tracking is the Extended Kalman Filter (EKF) [29], summarized in Algorithm 1. The 2-norm in Eq. (2-1) shows the measurement model for the UWB data is nonlinear. The EKF [30], [31], works similar to a Kalman Filter (KF), but is suitable for nonlinear state space models. The principle of EKF is that the nonlinear equation

is linearized around the current state estimate with first-order Taylor expansion. Therefore, the Jacobian matrix is calculated, which is then used in the equations of the Kalman Filter [32]. The EKF consists of a time update (prediction) and a measurement update (correction) [17], [31]. The time update uses a dynamic model to predict the current state based on the previous state estimate. In the case of position estimation, the time update can be calculated with the Constant Velocity Model (CVM) with state $x_t = (p_t,\ v_t)^\top$ [29]

$$x_t = \begin{bmatrix} I_{3\times3} & \Delta t \cdot I_{3\times3} \\ 0 & I_{3\times3} \end{bmatrix} x_{t-1} + \begin{bmatrix} \frac{(\Delta t)^2}{2} \cdot I_{3\times3} \\ \Delta t \cdot I_{3\times3} \end{bmatrix} w_{t-1}, \tag{2-10}$$

where $w_t \sim \mathcal{N}(0,\ \Sigma_{w,t})$ is the process noise and Δt the time between two UWB measurements. Once UWB measurements are available, the measurement update is performed. In this step, the state estimated from the time update is corrected with the linearization of the model in Eq. (2-1) [33]. This is the Jacobian of Eq. (2-1) with respect to the current state estimate. The measurement vector contains the range values for each anchor i. During the measurement update, the CVM model and UWB data are combined to mitigate NLOS errors in UWB measurements.

Algorithm 1 EKF with Constant Velocity Model (CVM) and UWB measurements [17],[29], [30], [31]

1: Perform an initialization on the state estimate and the covariance matrix.
2: Time update: Predict the current state and covariance matrix using the CVM model in Eq. (2-10).
3: Measurement update: If new UWB measurements are available, do a measurement update with outlier detection. Linearize the UWB model in Eq. (2-1) by computing the Jacobian matrix. Use the UWB measurements in combination with Eq. (2-1) to correct the state estimate from the previous step and update the covariance matrix.
4: Set $t := t + 1$ and iterate from Step 2.

Due to NLOS or multipath errors, the UWB measurements can contain a delay. These measurements can be detected in the measurement update step with hypothesis testing on the EKF's residuals [34], [17]. The residual is the difference between the measured UWB distance $y^i_{d,t}$ for anchor i and the predicted UWB distance $\hat{y}^i_{d,t}$. The predicted UWB distance $\hat{y}^i_{d,t}$ is calculated by substituting the position state estimate $\hat{p}_t$ resulting from the CVM model into the UWB measurement model Eq. (2-1). The residuals are normal distributed if there are no delays. Therefore, the normal distribution provides a confidence interval for the predicted UWB distances. When an anchor's residual is larger, the pdf value of this anchor is smaller [34]. If a measured UWB distance does not satisfy this interval, the measurement is detected as an outlier and therefore ignored [17].

Instead of using the Gaussian distribution to detect and mitigate NLOS outliers, a constant threshold can be used [12]. Let $r^i_t = |y^i_{d,t} - \hat{y}^i_{d,t}|$ be the absolute value of the residual. The NLOS judgement works according to the following formula:

$$\begin{cases} r^i_t \geq \nu,\ \text{NLOS} \\ r^i_t < \nu,\ \text{LOS} \end{cases}, \tag{2-11}$$

for some predefined threshold ν. In the case of $r_t^i \geq \nu$, the UWB measurement is being mitigated as outlier.

2-2-2 Position estimation with UWB and IMU

Previous research on UWB/IMU sensor fusion consists of Bayesian filtering, optimization, and machine learning methods. The machine learning methods in [35], [36] are considered too far from the current ways of working of Sendrato, and will therefore not be used in further research on this problem. The Bayesian filtering methods occurring in literature are the Extended Kalman Filter (EKF), Unscented Kalman Filter (UKF), and Particle Filter (PF) [8], [16], [37], [32], [38]. An EKF is commonly used in literature for UWB/IMU fusion [34], [17], [31], [33]. In Subsection 2-2-1 the EKF was described when only the UWB data was used. The time update consisted of a Constant Velocity Model (CVM) to predict the current state based on the previous state estimate. In Subsection 2-1-2 the dynamic model in Eq. (2-4) is derived that uses the IMU measurements as input. To fuse the data from the UWB and IMU sensors, the dynamic IMU model (2-4) can be used in the time update instead of a CVM. Once UWB measurements are available, the state estimate $\hat{x}_t = (p_t^n,\ v_t^n,\ q_t^{nb})^\top$ following from the dynamic IMU model is updated using the linearization of the UWB model in Eq. (2-1) [33]. During this measurement update, the dynamic IMU model and UWB data are combined to reduce NLOS errors in UWB measurements and integration drift in the IMU model. The EKF method for UWB/IMU sensor fusion is summarized in Algorithm 2.

Algorithm 2 EKF for UWB/IMU sensor fusion [17], [30], [31], [33], [34]

Initialize:
  State vector: $x_0 = (p_0,\ v_0,\ q_0)^\top$
  Covariance matrix: P_0
loop
  $t \leftarrow t + 1$
  $\hat{x}_t \leftarrow f(\hat{x}_{t-1},\ y_{a,t},\ y_{\omega,t},\ e_{a,t} = 0,\ e_{\omega,t} = 0)$ ▷ IMU measurements
  $P_t \leftarrow F_t P_{t-1} F_t^\top + G_t Q_{t-1} G_t^\top$
  $K_t \leftarrow P_t (H_t^{\text{UWB}})^\top (H_t^{\text{UWB}} P_t (H_t^{\text{UWB}})^\top + R_t^{\text{UWB}})^{-1}$
  $\hat{x}_t \leftarrow \hat{x}_t + K_t (y_{d,t} - H_t^{\text{UWB}} \hat{x}_t)$ ▷ UWB measurements
  $P_t \leftarrow (I - K_t H_t^{\text{UWB}}) P_t$
end loop

The function f is the dynamic IMU model given in Eq. (2-4). It uses the gyroscope and accelerometer measurements as inputs. The covariance is updated using the Jacobian matrices $F_t = \frac{\partial f}{\partial x}\Big|_{x=\hat{x}_{t-1}}$ and $G_t = \frac{\partial f}{\partial e}\Big|_{x=\hat{x}_{t-1}}$, with $\hat{x}$ the current state estimate. The process noise covariance of the time update step is denoted by Q_t. In the measurement update the UWB measurements are incorporated by calculating the Kalman gain K_t. The Kalman gain is calculated using the linearization of the measurement model in Eq. (2-1). Let $h_i(x_t, p_{\text{anc}}^i)$ be the function in Eq. (2-1); $y_{d,t}^i = h_i(x_t, p_{\text{anc}}^i) + e_{d,t}^i$. Then $H_t^{i,\text{UWB}} = \frac{\partial h_i}{\partial x}\Big|_{x=\hat{x}_t}$ is the Jacobian for each measurement. These are stacked vertically in the matrix H_t^{UWB}. Finally, $y_{d,t}$ is the vector with the ranging measurements from all anchors $y_{d,t}^i$ at time t. R_t^{UWB} is the

corresponding measurement noise covariance matrix.

A downside of the EKF that literature mentions is that linearization errors can occur because the Taylor expansion used for linearization only retains first order terms [37]. An UKF addresses this problem by using the Unscented Transformation for linearization without having to calculate Jacobian matrices [30], [39], [37], [16], [32]. However, some literature states that when the models are reasonably nonlinear, this method also adds unnecessary complexity [38]. The PF can be useful when the noise is non-gaussian [16], [30], [40]. However, the computational complexity increases with the number of particles, while using too few particles reduces accuracy [16], [38]. To conclude, the choice of Bayesian filtering technique for UWB/IMU sensor fusion requires balancing accuracy and computational complexity, and depends on the level of nonlinearity of the system. Furthermore, the distribution of the noise influences the choice of sensor fusion method. EKF and UKF work best with Gaussian noise. Literature also proposed to incorporate the NLOS and multipath errors in the UWB measurement model through a tailored heavy-tailed asymmetric distribution. The UWB and IMU measurements can then be fused by solving a Maximum a Posteriori (MAP) problem, which is an optimization problem [9]. There exist even more Bayesian filtering techniques for sensor fusion. However, all methods have similar workings and can be used with arbitrary models for the UWB and IMU measurements, as long as the noise distribution corresponds to the algorithm of choice. Additionally, literature exists that claims that Bayesian filtering techniques lead to underuse of information due to the Markov assumption. Instead, graph optimization is proposed, where the nodes represent the anchors and the tag at different time instances and the edges represent the measurements. These algorithms use a sliding trajectory window and maintain previous statuses [21], [40].

This thesis chooses to make minimal changes to Sendrato's current processes to use them as a baseline for improvement. Therefore, it is chosen to stay close to their current method of UWB-only tracking, which is the EKF. For this research, an EKF is examined that uses the IMU data for propagation of the state and the UWB data for state correction. The UWB/IMU EKF developed for this research will be explained in more detail in Chapter 3.

2-3 Previous research on fusion of two tags

The previous sections discussed background information and related work on position estimation with UWB data and UWB/IMU sensor fusion. This section discusses an additional method to compensate for the NLOS errors of the UWB system. That is to attach two UWB sensors on opposite sides of the user's body, to compensate for NLOS errors caused by the body blocking the UWB signals. Because these tags estimate the position of two different locations on the body, fusion methods are needed to combine the information from the two separate tags to estimate the location of the person. In the case of TraXYZ, the UWB tags are also equipped with an IMU sensor. Therefore, sensor fusion is needed for two UWB and two IMU sensors, whose data is also fused through UWB/IMU sensor fusion methods from the previous section. This section starts with previous research on sensor fusion of two IMUs attached to a person to track the person's location. This is described in Subsection 2-3-1.

Thereafter, Subection 2-3-2 describes previous research on sensor fusion of two UWB tags attached to the person.

2-3-1 Sensor fusion of two IMUs

Sensor fusion of multiple IMUs is often researched to prevent heading drift. This means that the estimated track increasingly drifts away from the true path over time, which is mainly the problem when tracking a pedestrian with two foot-mounted IMUs [41]. A way to mitigate heading drift in pedestrian tracking is to attach more than one IMU [41], [15], [42]. The sensor fusion is then based on knowledge of the relative distance between the foot-mounted IMUs when the person is walking. Two methods to implement this relative distance are: the maximum relative distance and the spacing vector constraint. The main idea is to project the estimate that is influenced by heading drift back to the space bordered by the maximum possible relative distance.

In the case of a pedestrian with two foot-mounted IMUs, the relative distance between the IMUs is not fixed while walking. Therefore, it becomes challenging to relate the position estimates of both IMUs to each other. However, there exists an upper bound on how large the distance between the two can be. This is called the maximum relative distance. Let the joint state estimate of sensor 1 and 2 be

$$\hat{x}_t = [(\hat{x}_t^{(1)})^\top \ (\hat{x}_t^{(2)})^\top]^\top \tag{2-12}$$

and suppose the first s elements of $\hat{x}_t^{(m)} \in \mathbb{R}^{n_m}$, $m = 1, 2$, represent position, with s is 2 or 3. Prior knowledge of the maximum relative distance γ imposes a constraint on the joint state estimate that can be formulated as [15]

$$\|L\hat{x}_t\|^2 \leq \gamma^2. \tag{2-13}$$

with $L = [I_{s\times s} \ \ 0_{s,n_1-s} \ \ -I_{s\times s} \ \ 0_{s,n_2-s}]$. When $\|L\hat{x}_t\|^2 > \gamma^2$ the joint state estimate should be projected to the space $\{x \in \mathbb{R}^{n_1+n_2} \|Lx\|^2 \leq \gamma^2\}$. The projection $\rho(\hat{x}_t)$ is the result of an inequality constrained weighted least squares problem:

$$\rho(\hat{x}_t) = \arg\min_x (\|\hat{x}_t - x\|^2_{P_t^{-1}}) \quad \text{s.t.} \quad \|Lx\|^2 \leq \gamma^2, \tag{2-14}$$

where P_t is the covariance matrix of $\hat{x}_t$. The optimization problem in Eq. (2-14) is solved by finding the stationary point of the Lagrange function with the help of, for example, the Bisection method or Newton's method [15]. The covariance of the projected joint state estimate P_t^* is approximated as [15]

$$P_t^* = \nabla\rho P_t (\nabla\rho)^\top, \tag{2-15}$$

where $\nabla\rho$ is the Jacobian of the projection function $\rho(x)$ with respect to x evaluated at $\hat{x}_t$. If the joint state estimate $\hat{x}_t$ exceeds constraint Eq. (2-13), then $\hat{x}_t$ is updated with the projection in Eq. (2-14) and the covariance matrix is updated with Eq. (2-15).

Furthermore, a fixed distance between the IMUs can be considered in the fusion method, instead of a maximum relative distance. The fixed distance can be implemented with the 'spacing vector constraint' [42]. The method in [42] assumes that the distance between the

IMUs is fixed each time the feet are side by side during a leg swing. The proposed constraint only applies at these moments while walking, to prevent the estimated IMU positions from crossing each other (the left IMU stays left and the right stays right). However, when the IMUs are placed on the hips, this constraint can apply at all times. Suppose the distance between the IMUs is the now fixed value γ. This can be expressed as the equality constraint [42]

$$L\hat{x}_t = R(\psi_t) \begin{bmatrix} \gamma \\ 0 \end{bmatrix} \in \mathbb{R}^s, \tag{2-16}$$

with L defined in Eq. (2-13), and $s = 2$ in this case. ψ_t is the circular average of the two heading angles of the IMUs

$$\psi_t = \arctan \frac{\sin \psi_t^{(1)} + \sin \psi_t^{(2)}}{\cos \psi_t^{(1)} + \cos \psi_t^{(2)}}. \tag{2-17}$$

The matrix $R(\psi_t)$ is a rotation matrix that rotates the position around an axis through angle ψ_t. For the two-dimensional position, $R(\psi_t)$ is given as

$$R(\psi_t) = \begin{bmatrix} \cos \psi_t & -\sin \psi_t \\ \sin \psi_t & \cos \psi_t \end{bmatrix}. \tag{2-18}$$

Taking the squared Euclidean norm of both sides in Eq. (2-16) results in the constraint of Eq. (2-13) when this is changed into an equality constraint. Let the right-hand-sight of Eq. (2-16) be denoted by $\mu \in \mathbb{R}^s$. The projection $\rho(\hat{x}_t)$ is given by

$$\rho(\hat{x}_t) = \arg\min_x (\|\hat{x}_t - x\|^2_{P_t^{-1}}) \quad \text{s.t.} \quad Lx = \mu. \tag{2-19}$$

With known solution [43]

$$\rho(\hat{x}_t) = \hat{x}_t - P_t L^T (L P_t L^T)^{-1} (L\hat{x}_t - \mu). \tag{2-20}$$

2-3-2 Sensor fusion of two UWB tags

Relatively few literature is found on sensor fusion of multiple UWB tags placed on a single object to be tracked. However, [44] presents a method to fuse two UWB tags placed on both sides of the object based on the known distance between the tags. In the end, the fused position from the UWB tags is fused with data from a built-in IMU of the object, in a loosely coupled fashion. First, initial tag position estimates $p_{\text{tag}}^{(1)}$, $p_{\text{tag}}^{(2)}$ are calculated by applying a Non-Linear Least Squares (NLS) calculation on Kalman filtered UWB measurements. Secondly, these initial estimates are fused based on a cost function [44]

$$J\left(p_{\text{tag}}^{(1)}, p_{\text{tag}}^{(2)}, \gamma\right) = \arg\min_{p_{\text{tag}}^{(m)}} \left(200 \left(\|p_{\text{tag}}^{(1)} - p_{\text{tag}}^{(2)}\|^2 - \gamma^2 \right)^2 + \sum_{m,i} \left(\|p_{\text{tag}}^{(m)} - p_{\text{anc}}^{i}\|^2 - (y_{d,t}^{i,(m)})^2 \right)^2 \right), \tag{2-21}$$

where $m \in \{1, 2\}$ indicates the UWB tag, i indicates the UWB anchor and $p_{\text{tag}}^{(1)}$, $p_{\text{tag}}^{(2)}$ are the tag locations resulting from a Non-Linear Least Squares (NLS) calculation using preprocessed UWB measurements. Furthermore, $y_{d,t}^{i,(m)}$ is the measured distance between UWB tag

m and anchor i. Because the value of γ is known and fixed, the first term in Eq. (2-21) is given a large weight of 200. Hence, the cost function ensures that the estimated tag positions meet the distance measurements while, most importantly, the distance between the tags remains as close to γ as possible. The numerical problem is solved using gradient descent.

Chapter 3

Methodology

This chapter provides an overview of the methods developed and implemented for analyzing the effects of UWB/IMU sensor fusion and the fusing of the two tags worn on the individual's hips. It is chosen to implement an EKF to estimate the artist's position, because this algorithm is commonly used in literature for UWB/IMU sensor fusion, as discussed in the previous chapter, and the EKF is close to the current ways of working of Sendrato. The algorithm developed for this thesis is presented in Algorithm 3. This chapter explains how this algorithm is built and explains each component of the EKF in detail. Algorithm 3 will be explained in two parts. Section 3-1 focuses on UWB/IMU sensor fusion for each tag (Subsection 3-1-1), where additional components are added and later analyzed on their potential for improving tracking accuracy. These additional components are bias estimation and correction (Subsection 3-1-2), a Zero Velocity Update (ZUPT) (Subsection 3-1-3), and Non-Line-of-Sight (NLOS) detection and mitigation (Subsection 3-1-4). The second part of the algorithm, Section 3-2, explains the developed method for the tightly coupled sensor fusion of the two tags on the hips, based on the known distance between the tags. This method is then implemented into the UWB/IMU sensor fusion EKF of Section 3-1. The structure of Algorithm 3 allows for analyzing the effects of the different components and combinations thereof, including fusing the two tags, where the baseline is the UWB/IMU sensor fusion method for loosely coupled tags in Subsection 3-1-1. Section 3-3 presents the resulting final algorithm developed for this research in more detail. Ultimately, this research compares the results of all methods in this chapter to the UWB-only EKF for loosely coupled tags baseline from Subsection 2-2-1.

Algorithm 3 Tightly coupled EKF for UWB/IMU sensor fusion and fusion of two tags

Initialize:
Joint state vector: $x_0 = [(x_0^{(1)})^\top \ (x_0^{(2)})^\top]^\top$, with $x_0^{(m)}$ the state of tag $m \in \{1, 2\}$
Covariance matrix: P_0
loop
  $t \leftarrow t + 1$
  if doBIAS **then**
    Include the methods from Subsection 3-1-2. EKF time update: Predict the current state and covariance matrix using the IMU measurements and the dynamic IMU model in Eq. (2-4). The measurements are corrected for bias.
  else
    EKF time update: Predict the current state and covariance matrix using the IMU measurements and the dynamic IMU model in Eq. (2-4).
  end if
  if doZUPT **then**
    Include the Zero Velocity Update (ZUPT) described in Subsection 3-1-3. If the ZUPT detector detects a stationary point, update the velocity estimate to zero.
  end if
  if doNLOS **then**
    Include the Non-Line-of-Sight (NLOS) methods described in Subsection 3-1-4. If NLOS is detected the UWB measurement is rejected.
  end if
  if doJOIN **then**
    Include the method for fusing the two tags described in Section 3-2. EKF measurement update: Correct the current state estimate using the UWB measurements and the measurement model in Eq. (2-1), and knowledge of the relative distance between the tags.
  else
    EKF measurement update: Correct the current state estimate using the UWB measurements and the measurement model in Eq. (2-1).
  end if
end loop

3-1 UWB/IMU sensor fusion

3-1-1 UWB/IMU sensor fusion with EKF

Subsection 2-2-2 described a general EKF for UWB/IMU fusion. Ultimately, the goal is to also fuse the data from the two tags on the hips. Inspired by Subsection 2-3-1, a joint state vector $x_t = [(x_t^{(1)})^\top \ (x_t^{(2)})^\top]^\top$, with $x_t^{(m)} = [p_t, \ v_t, \ q_t]^\top$ for tag $m \in \{1, 2\}$, is defined for Tag1 and Tag2 of this experiment considering that ultimately the tags will be fused in a tightly coupled fashion. This section describes the EKF where the two tags are yet loosely coupled, while the two tag states are combined into one state vector. The use of a joint state vector alters the general EKF in Algorithm 2 to the EKF in Algorithm 4 of this section. The algorithm iterates through all time instances where at least one sensor provides data. However, the measurements should be used for the state estimate of only the corresponding

tag. Therefore, the time update in lines 4-18 of Algorithm 4 is separated into two if-statements for the tags. Each if-statement considers Δt as the time difference between the current t and the previous time instance when data was obtained from the corresponding tag. Δt enters the algorithm in the state prediction in line 5 and 16. Let $F_t^{(m)}$ and $G_t^{(m)}$ be the Jacobians corresponding to the state and error of tag $m \in \{1, 2\}$, respectively. The expressions for $F_t^{(m)}$ and $G_t^{(m)}$ are given in Eq. (A-1) and Eq. (A-2) in Appendix A. Furthermore, let

$$P_t^* \coloneqq \begin{bmatrix} F_t^{(1)} & 0 \\ 0 & I_{n_2 \times n_2} \end{bmatrix} P_{t-1} \begin{bmatrix} F_t^{(1)} & 0 \\ 0 & I_{n_2 \times n_2} \end{bmatrix}^\top + \begin{bmatrix} G_t^{(1)} & 0 \\ 0 & 0 \end{bmatrix} \begin{bmatrix} Q_{t-1}^{(1)} & 0 \\ 0 & 0 \end{bmatrix} \begin{bmatrix} G_t^{(1)} & 0 \\ 0 & 0 \end{bmatrix}^\top. \tag{3-1}$$

It can be proven that

$$\begin{aligned} &F_t P_{t-1} F_t^\top + G_t Q_{t-1} G_t^\top \\ &= \begin{bmatrix} F_t^{(1)} & 0 \\ 0 & F_t^{(2)} \end{bmatrix} P_{t-1} \begin{bmatrix} F_t^{(1)} & 0 \\ 0 & F_t^{(2)} \end{bmatrix}^\top + \begin{bmatrix} G_t^{(1)} & 0 \\ 0 & G_t^{(2)} \end{bmatrix} \begin{bmatrix} Q_{t-1}^{(1)} & 0 \\ 0 & Q_{t-1}^{(2)} \end{bmatrix} \begin{bmatrix} G_t^{(1)} & 0 \\ 0 & G_t^{(2)} \end{bmatrix}^\top \\ &= \begin{bmatrix} I_{n_1 \times n_1} & 0 \\ 0 & F_t^{(2)} \end{bmatrix} P_t^* \begin{bmatrix} I_{n_1 \times n_1} & 0 \\ 0 & F_t^{(2)} \end{bmatrix}^\top + \begin{bmatrix} 0 & 0 \\ 0 & G_t^{(2)} \end{bmatrix} \begin{bmatrix} 0 & 0 \\ 0 & Q_{t-1}^{(2)} \end{bmatrix} \begin{bmatrix} 0 & 0 \\ 0 & G_t^{(2)} \end{bmatrix}^\top \end{aligned} \tag{3-2}$$

by writing out the bottom line. It also follows from the dynamic models for the separate tags, where consecutively $x_t^{(2)} = x_{t-1}^{(2)}$ and $x_t^{(1)} = x_{t-1}^{(1)}$. Taking the Jacobians of these equations explains the I and 0 elements of F_t and G_t. The theory of Eq. (3-2) allows a time update at time instances where data is obtained from only one of the two IMU sensors, but also works when both sensors provide data simultaneously. For the measurement update with UWB data in lines 19-23, all UWB measurements of both tags are combined in one measurement vector $y_{d,t} = \begin{bmatrix} y_t^{(1)} \\ y_t^{(2)} \end{bmatrix}$. These are modelled with the measurement Jacobian

$$H_t^{\text{UWB}} = \begin{bmatrix} H_t^{(1),\text{UWB}} & 0 \\ 0 & H_t^{(2),\text{UWB}} \end{bmatrix} \in \mathbb{R}^{\#y_{d,t} \times (n_1 + n_2)}, \tag{3-3}$$

with n_1, n_2 the lengths of $x_t^{(1)}$ and $x_t^{(2)}$, respectively. The expression for $H_t^{(m),\text{UWB}}$ for tag $m \in \{1, 2\}$ is given in Eq. (A-3) in Appendix A. The measurement noise covariance matrix is

$$R_t^{\text{UWB}} = \begin{bmatrix} R_t^{(1),\text{UWB}} & 0 \\ 0 & R_t^{(2),\text{UWB}} \end{bmatrix} \in \mathbb{R}^{\#y_{d,t} \times \#y_{d,t}}. \tag{3-4}$$

Initialization

The initial position p_0^n in the navigation frame can be approximated based on the UWB measurements or knowledge of the starting position at the beginning of the experiment. With the UWB data at time zero, the initial position in the navigation frame can be calculated using multilateration or NLS. When the person's starting point relative to one or more anchor

Algorithm 4 EKF for UWB/IMU sensor fusion with loosely coupled tags

Initialize:
  Joint state vector: $x_0 = [(x_0^{(1)})^\top \ (x_0^{(2)})^\top]^\top$,
  with $x_0^{(m)} = [p_0,\ v_0,\ q_0]^\top$ for tag $m \in \{1, 2\}$
  Covariance matrix: P_0
loop
  $t \leftarrow t + 1$
  if $y_{a,t}^{(1)},\ y_{\omega,t}^{(1)}$ **then** ▷ IMU measurements
    $\hat{x}_t^{*(1)} \leftarrow f(\hat{x}_{t-1}^{(1)},\ y_{a,t}^{(1)},\ y_{\omega,t}^{(1)},\ e_{a,t}^{(1)} = 0,\ e_{\omega,t}^{(1)} = 0)$
    $\hat{x}_t^{(2)} \leftarrow \hat{x}_{t-1}^{(2)}$
    $P_t^* \leftarrow \begin{bmatrix} F_t^{(1)} & 0 \\ 0 & I_{n_2 \times n_2} \end{bmatrix} P_{t-1} \begin{bmatrix} F_t^{(1)} & 0 \\ 0 & I_{n_2 \times n_2} \end{bmatrix}^\top + \begin{bmatrix} G_t^{(1)} & 0 \\ 0 & 0 \end{bmatrix} \begin{bmatrix} Q_{t-1}^{(1)} & 0 \\ 0 & 0 \end{bmatrix} \begin{bmatrix} G_t^{(1)} & 0 \\ 0 & 0 \end{bmatrix}^\top$
    $\hat{x}_t^{(1)} \leftarrow \hat{x}_t^{*(1)}$
    $P_t \leftarrow P_t^*$
  else
    $\hat{x}_t^{*(1)} \leftarrow \hat{x}_{t-1}^{(1)}$
    $P_t^* \leftarrow P_{t-1}$
  end if
  if $y_{a,t}^{(2)},\ y_{\omega,t}^{(2)}$ **then** ▷ IMU measurements
    $\hat{x}_t^{(1)} \leftarrow \hat{x}_t^{*(1)}$
    $\hat{x}_t^{(2)} \leftarrow f(\hat{x}_{t-1}^{(2)},\ y_{a,t}^{(2)},\ y_{\omega,t}^{(2)},\ e_{a,t}^{(2)} = 0,\ e_{\omega,t}^{(2)} = 0)$
    $P_t \leftarrow \begin{bmatrix} I_{n_1 \times n_1} & 0 \\ 0 & F_t^{(2)} \end{bmatrix} P_t^* \begin{bmatrix} I_{n_1 \times n_1} & 0 \\ 0 & F_t^{(2)} \end{bmatrix}^\top + \begin{bmatrix} 0 & 0 \\ 0 & G_t^{(2)} \end{bmatrix} \begin{bmatrix} 0 & 0 \\ 0 & Q_{t-1}^{(2)} \end{bmatrix} \begin{bmatrix} 0 & 0 \\ 0 & G_t^{(2)} \end{bmatrix}^\top$
  end if
  if $y_{d,t}$ **then**
    $K_t \leftarrow P_t (H_t^{\text{UWB}})^\top (H_t^{\text{UWB}} P_t (H_t^{\text{UWB}})^\top + R_t^{\text{UWB}})^{-1}$
    $\hat{x}_t \leftarrow \hat{x}_t + K_t (y_{d,t} - H_t^{\text{UWB}} \hat{x}_t)$ ▷ UWB measurements
    $P_t \leftarrow (I - K_t H_t^{\text{UWB}}) P_t$
  end if
end loop

positions is known, the initial coordinates can also be estimated based on the approximate distance to the known anchor coordinates. The initial z-coordinate can be measured beforehand. The initial velocity is set to zero. Finally, the initial orientation can be calculated using the accelerometer measurements at time zero. Literature in [13] explains a method for estimating initial orientation using the first accelerometer and magnetometer measurements. However, magnetometer measurements are unavailable in the context of this research. Magnetometer measurements provide information about the heading. Hence without magnetomer measurements, this method can approximately determine initial inclination, but initial heading can not follow from this method. To obtain an indication of initial orientation, the method in

[13] is adjusted for this research. Define the four normalized vectors [13]

$$\hat{g}^n = (0\ 0\ 1)^\top, \quad \hat{g}^b = \frac{y_{a,0}}{\|y_{a,0}\|_2}, \tag{3-5a}$$

$$\hat{m}^n = (0\ 1\ 0)^\top, \quad \hat{m}^b = \hat{g}^b \times \left(\hat{m}^b \times \hat{g}^b\right). \tag{3-5b}$$

These vectors represent the gravity vector in the navigation frame and the body frame (i.e. the sensor frame of the IMU), and the magnetic field vector in the navigation frame and the body frame. The calculation of $\hat{m}^b$ in Eq. (3-5b) originally uses the normalized magnetometer measurements in the body frame. Due the lack of magnetometer measurements, $\hat{m}^b$ is set equal to $\hat{m}^n$. The initial orientation q_0^{nb} is the solution to an optimization problem that finds the orientation that minimizes the distance between the gravity vector and the normalized magnetic field vector in the navigation frame ($\hat{g}^n$, $\hat{m}^n$) and the gravity vector following from the first accelerometer data ($\hat{g}^b$) and the magnetic field vector in the body frame, where $\hat{m}^b = \hat{m}^n$. The optimization problem leads to the matrix

$$A = -(\bar{\hat{g}}^n)^L(\bar{\hat{g}}^b)^R - (\bar{\hat{m}}^n)^L(\bar{\hat{m}}^b)^R. \tag{3-6}$$

$\bar{x}^n = (0\ (x^n)^\top)^\top$ denotes the quaternion representation of an arbitrary vector x^n. Then,

$$(\bar{x}^n)^L \coloneqq \begin{bmatrix} \bar{x}_0 & -(\bar{x}_n)^\top \\ \bar{x}_n & \bar{x}_0 I_{3\times 3} + [\bar{x}_n\times] \end{bmatrix} \text{ and } (\bar{x}^n)^R \coloneqq \begin{bmatrix} \bar{x}_0 & -(\bar{x}_n)^\top \\ \bar{x}_n & \bar{x}_0 I_{3\times 3} - [\bar{x}_n\times] \end{bmatrix}, \tag{3-7}$$

where

$$[\bar{x}_n\times] \coloneqq \begin{bmatrix} 0 & -x_3^n & x_2^n \\ x_3^n & 0 & -x_1^n \\ -x_2^n & x_1^n & 0 \end{bmatrix}. \tag{3-8}$$

The solution for q_0^{nb} is given by the eigenvector corresponding to the largest eigenvalue of A [13]. Since the measured UWB distances can indicate the walking direction, the initial heading will be corrected once UWB measurements are inserted in the EKF.

3-1-2 Bias estimation

There are two ways to account for bias included in the accelerometer and gyroscope measurements. The first is to subtract a constant bias from the measurements before being substituted into the dynamic model. Leaving the sensor stationary for some time can indicate the magnitude of the constant bias. For the gyroscope, it is expected that the measurements in all axes give zero. In case of bias, the mean of the data is nonzero. The mean can be used as the value for the constant gyroscope bias $\delta_{\omega,t}$ present in the sensor [13]. Determining the accelerometer bias $\delta_{a,t}$ is less straightforward. When the sensor is stationary, it is expected that the measurements give $(0\ 0\ 9.81)^\top$. If the measurement mean is larger than zero in the x- and/or y-axis, it does not necessarily indicate a bias. It could be that the surface is not completely flat, hence part of the gravity is "leaking" into the x- and y-axis. If the mean in the z-axis is larger than 9.81, this can indicate a bias at least in the z-axis [13].

The second way to address bias is to include $\delta^b_{\omega,t}$ and $\delta^b_{a,t}$ in the state vector and estimate their values with the EKF. The state is augmented to $x_t = (p^n_t,\ v^n_t,\ q^{nb}_t,\ \delta^b_{a,t},\ \delta^b_{\omega,t})^\top$. The dynamic model f in Eq. (2-4) used in the EKF time update is extended with the random walks

$$\delta^b_{a,t+1} = \delta^b_{a,t} + e^b_{\delta_a,t}, \tag{3-9a}$$

$$\delta^b_{\omega,t+1} = \delta^b_{\omega,t} + e^b_{\delta_\omega,t}, \tag{3-9b}$$

and the estimated bias states are subtracted from the IMU measurement input. The terms $e^b_{\delta_a,t}$ and $e^b_{\delta_\omega,t}$ are Gaussian noise terms and determine how constant the bias will be. The process noise of Eq. (3-9) is incorporated in the EKF process noise covariance matrix Q_t. The process noise covariance corresponding to Eq. (3-9) should be small to ensure the bias changes slowly over time and remains nearly constant. The initial bias can be set to zero, and subsequently, it can be checked if the estimated bias will converge over time, provided that the bias model process noise is set small. If the bias is included in the state vector and f is augmented with Eq. (3-9), it should also be factored into the calculation of the Jacobian for $F_t = \frac{\partial f}{\partial x}\Big|_{x=\hat{x}_{t-1}}$ and $G_t = \frac{\partial f}{\partial e}\Big|_{x=\hat{x}_{t-1}}$. This means the matrices F_t and G_t increase dimension. The expressions for F_t and G_t adjusted for bias estimation are given in Eq. (A-4) to Eq. (A-6) in Appendix A.

3-1-3 Zero velocity update (ZUPT)

In UWB/IMU sensor fusion techniques, the IMU measurements are not only able to suppress NLOS errors, but the measurements can also be used to prevent sensor drift over time [45]. When the person is stationary, the velocity estimate is expected to be zero. This idea can be used to correct state estimates during the period the person's velocity and angular velocity are close to zero [46]. The goal of a Zero Velocity Update (ZUPT), is to detect when the IMU is stationary and subsequently correct the velocity estimate to zero. The ZUPT functions therefore as a pseudo-measurement inserted in a measurement update of an EKF [45].

The first step is to detect the stationary state with a binary hypothesis testing problem [47]. Let $z_{a,n} \coloneqq \{y_{a,t}\}_{t=n}^{n+N-1}$ and $z_{\omega,n} \coloneqq \{y_{\omega,t}\}_{t=n}^{n+N-1}$ denote the IMU measurement sequences during a time epoch consisting of $N \in \mathbb{N}$ measurements between time instants n and $n+N-1$. Then the detector decides that the IMU is stationary if

$$T(z_{a,n}, z_{\omega,n}) < \text{Thr}. \tag{3-10}$$

This is the binary hypothesis testing problem consisting of the test statistics $T(z_{a,n}, z_{\omega,n})$ and the detection threshold Thr. This research uses a Stance Hypothesis Optimal Detector (SHOD) defined as [47]

$$T(z_{a,n}, z_{\omega,n}) = \frac{1}{N}\sum_{t=n}^{n+N-1} \frac{1}{\sigma_a^2}\|y_{a,t} - g\frac{\bar{y}_{a,n}}{\|\bar{y}_{a,n}\|}\|^2 + \frac{1}{\sigma_\omega^2}\|y_{\omega,t}\|^2, \tag{3-11}$$

where $\bar{y}_{a,n} = \frac{1}{N}\sum_{t=n}^{n+N-1} y_{a,t}$ denotes the sample mean, σ_a^2 and σ_ω^2 denote the variance of the acceleration noise and angular velocity noise, respectively, and g is the gravitational acceleration.

During the time period in which the IMU is detected stationary according to Eq. (3-10), the state propagated by the dynamic IMU model is corrected using the Kalman gain for the ZUPT model. The pseudo-measurements used for the ZUPT update $y_{\text{zupt},t}$ are modeled as [41]

$$y_{\text{zupt},t} = H_t^Z x_t + e_{Z,t}, \tag{3-12}$$

with H_t^Z the observation matrix that has ones in the elements corresponding to velocity and zeros in the other elements, and $e_{Z,t}$ the process noise. During the time that Eq. (3-10) is valid, in each iteration the estimated state $\hat{x}_t$ is corrected by the ZUPT measurement through the equation $\hat{x}_t \leftarrow \hat{x}_t - K_t H_t^Z \hat{x}_t$ with K_t the Kalman gain, which is calculated similarly as in Algorithm 2 [41].

The algorithm is tuned by adjusting the values for the horizon N, the ratio of the noise variances the ratio $\sigma_a^2/\sigma_\omega^2$, and the threshold Thr. If the stationary points in the trajectory are known, it can be verified if only these points are detected as zero velocity points. If not, the algorithm can be tuned accordingly.

The ZUPT algorithm to be implemented in the EKF of Algorithm 4 is summarized in Algorithm 5. The detector T detects if one of the two tags is considered stationary. It is assumed that the other tag is then also stationary, since the tags are placed on the hips. The "and" statement is used as additional assurance that the person is stationary and prevents that one tag detects false stationary points. The ZUPT matrices are defined as

$$H_t^Z = \begin{bmatrix} H_t^{(1),Z} & 0 \\ 0 & H_t^{(2),Z} \end{bmatrix} \in \mathbb{R}^{6\times \#states} \tag{3-13}$$

and $H_t^{(m),Z}$is the matrix with ones in the elements corresponding to velocity and zeros in the other elements. The noise covariance matrix is the 6×6 matrix R_t^Z that has $R_t^{(1),Z}$ and $R_t^{(2),Z}$ on its diagonal.

Algorithm 5 ZUPT algorithm for two tags

if $T(z_{a,n}^{(1)},\ z_{\omega,n}^{(1)}) <$ Thr and $T(z_{a,n}^{(2)},\ z_{\omega,n}^{(2)}) <$ Thr **then** ▷ ZUPT detector
  $K_t \leftarrow P_t (H_t^Z)^\top \left(H_t^Z P_t (H_t^Z)^\top + R_t^Z \right)^{-1}$
  $\hat{x}_t \leftarrow \hat{x}_t - K_t H_t^Z \hat{x}_t$
  $P_t \leftarrow (I - K_t H_t^Z) P_t$
end if

3-1-4 NLOS detection and mitigation with IMU data

Section 2-2 discussed two ways for mitigating the delay in the UWB ranging measurements due to NLOS: a constant threshold on the absolute value of the residual $r_t^i = |y_{d,t}^i - \hat{y}_{d,t}^i|$ and a confidence interval for the normal distribution. The methods both use the predicted UWB distance $\hat{y}_{d,t}^i$, which was calculated by substituting the position state estimate $\hat{p}_t$ resulting from the CVM model into the UWB measurement model Eq. (2-1). Instead of the CVM model, the dynamic IMU model in Eq. (2-4) is used to predict the state and therefore $\hat{y}_{d,t}^i$. For the

first method, a constant threshold can be set as in Eq. (2-11). This threshold should not be too small, since too many UWB measurements will be rejected for the estimated trajectory to be accurate. On the other hand, if the threshold is too large, too many inaccurate UWB measurements will be taken into the estimation algorithm. The second method, given in Algorithm 6, makes use of the fact that in the absence of measurement delays, the residuals are normal distributed according to [23]

$$y_{d,t} - \hat{y}_{d,t} \sim \mathcal{N}(0, S_t), \tag{3-14}$$

where $S_t = H_t^{\text{UWB}} P_t (H_t^{\text{UWB}})^\top + R_t^{\text{UWB}}$, and $y_{d,t}$ and $\hat{y}_{d,t}$ are vectors containing the distance measurements from each anchor, and the estimated distances from each anchor, respectively. P_t is the covariance matrix after the prediction step. Each independent ranging measurement in the vector $y_{d,t}$ needs to be checked if it is close to the predicted distance for that anchor, as some measurements may contain NLOS and some may not. Assume the measurements are uncorrelated, then for each measurement $y_{d,t}^i$ a confidence interval can be calculated using Eq. (3-14)

$$(CI)_i = c\sqrt{(S_t)_{ii}}, \tag{3-15}$$

with c the critical value corresponding to the desired confidence level. If $y_{d,t}^i - \hat{y}_{d,t}^i$ is not included in the interval $[-(CI)_i,\ (CI)_i]$, then this measurement is considered NLOS and rejected. Using this method avoids having to choose a random threshold.

Algorithm 6 NLOS mitigation with normal distribution confidence interval

if $y_{d,t}$ **then** ▷ UWB measurements
  $S_t \leftarrow H_t^{\text{UWB}} P_t (H_t^{\text{UWB}})^\top + R_t^{\text{UWB}}$
  $CI \leftarrow c\sqrt{diag(S_t)}$
  $y_{d,t} \leftarrow \left(y_{d,t}^i |\ y_{d,t}^i - \hat{y}_{d,t}^i \in [-(CI)_i, (CI)_i]\right)$ ▷ NLOS mitigation
  $H_t^{\text{UWB}},\ R_t^{\text{UWB}} \leftarrow \left[(H_t^{\text{UWB}})_i,\ (R_t^{\text{UWB}})_i |\ y_{d,t}^i - \hat{y}_{d,t}^i \in [-(CI)_i, (CI)_i]\right]$
end if

3-2 Fusion of two UWB/IMU tags

From the related work on the fusion of two tags in Section 2-3 it could be concluded that the sensor fusion of two UWB/IMU tags has not yet been researched extensively. Previous research primarily focused on two IMUs placed on the feet. For this thesis, a different situation applies where two tags equipped with both a UWB and an IMU sensor are placed on the hips. Therefore, the problem requires a fixed relative distance between the tags, unlike tags placed on the feet. In this section, the methods from previous research in Section 2-3 are adjusted for the methodology of this research problem; a fixed relative tag distance and an EKF. The methods described in Section 3-2 prompted the idea to enforce a fixed distance between the two UWB/IMU tags with an equality constraint on the joint state vector $x_t = \left[\left(x_t^{(1)}\right)^\top \ \left(x_t^{(2)}\right)^\top\right]^\top$. Hence for this research, an equality constraint needs to be included in an EKF. To include any equality constraint in an EKF, the equations in the EKF measurement update can be augmented with perfect measurements containing zero measurement noise [43]. This results in an unconstrained problem where the EKF state estimate

automatically satisfies the constraint.

The relative distance between the tags $\gamma \in \mathbb{R}$ is known and fixed. Let the joint state estimate of tags 1 and 2 be

$$\hat{x}_t = \left[\left(\hat{x}_t^{(1)} \right)^\top \quad \left(\hat{x}_t^{(2)} \right)^\top \right]^\top. \tag{3-16}$$

Then the equality constraint is formed as

$$\|L\hat{x}_t\|_2 = \gamma, \tag{3-17}$$

with $L = [I_{3\times 3} \;\; 0_{3,n_1-3} \;\; -I_{3\times 3} \;\; 0_{3,n_2-3}]$ and $n_1,\ n_2$ the size of the state vectors of Tag1 and Tag2. Eq. (3-17) is equivalent to the constraint in Eq. (2-16) when taking the Euclidean norm of both sides of that equation. Eq. (2-16) is a linear constraint. The constraint in Eq. (3-17) can also be linearized to

$$H_t^L \hat{x}_t = \gamma, \tag{3-18}$$

where H_t^L is the Jacobian of $\|Lx\|_2$ evaluated at $x = \hat{x}_t$. The expression for H_t^L is given in Eq. (A-7) in Appendix A. To ensure that the EKF estimates satisfy the constraint in Eq. (3-17), the EKF measurement update is augmented as

$$\begin{bmatrix} y_{d,t} \\ \gamma \end{bmatrix} = \begin{bmatrix} H_t^{\text{UWB}} \\ H_t^L \end{bmatrix} x_t + \begin{bmatrix} e_{d,t} \\ 0 \end{bmatrix}. \tag{3-19}$$

Then the relative distance γ is considered a perfect measurement containing zero noise. This results in an unconstrained problem where the EKF state estimate automatically satisfies $\|L\hat{x}_t\|_2 = \gamma$. Alternatively, the relative distance between the tags can be considered a soft constraint, meaning that the equality constraint is approximately satisfied rather than exactly satisfied [43]. This can be accomplished by adding noise to the "perfect" measurements in Eq. (3-19). The measurement equation augmentation method in Eq. (3-19) is similar to the projection method in Eq. (2-19), because the solution in Eq. (2-20) resembles the EKF measurement update in lines 3 and 7 of Algorithm 7. This algorithm shows how the EKF measurement update for loosely coupled tags in Algorithm 4 alters when the fixed distance constraint is included for tightly coupling the tags. Algorithm 7 replaces lines 19-23 of Algorithm 4 when the tags need to be tightly coupled. Lines 6-8 in Algorithm 7 enforce the fixed tag distance also when no UWB measurements are available.

Algorithm 7 Measurement update of the EKF for UWB/IMU sensor fusion with tightly coupled tags

if $y_{d,t}$ **then** ▷ UWB measurements

$K_t \leftarrow P_t \begin{bmatrix} H_t^{\text{UWB}} \\ H_t^L \end{bmatrix}^\top \left(\begin{bmatrix} H_t^{\text{UWB}} \\ H_t^L \end{bmatrix} P_t \begin{bmatrix} H_t^{\text{UWB}} \\ H_t^L \end{bmatrix}^\top + \begin{bmatrix} R_t^{\text{UWB}} & 0 \\ 0 & R_t^L \end{bmatrix} \right)^{-1}$ ▷ Include γ

$\hat{x}_t \leftarrow \hat{x}_t + K_t \left(\begin{bmatrix} y_{d,t} \\ \gamma \end{bmatrix} - \begin{bmatrix} H_t^{\text{UWB}} \\ H_t^L \end{bmatrix} \hat{x}_t \right)$

$P_t \leftarrow \left(I - K_t \begin{bmatrix} H_t^{\text{UWB}} \\ H_t^L \end{bmatrix} \right) P_t$

else

$K_t \leftarrow P_t (H_t^L)^\top \left(H_t^L P_t (H_t^L)^\top + R_t^L \right)^{-1}$

$\hat{x}_t \leftarrow \hat{x}_t + K_t(\gamma - H_t^L \hat{x}_t)$ ▷ Relative distance correction

$P_t \leftarrow (I - K_t H_t^L) P_t$

end if

3-3 Final algorithm

In Section 3-1 and 3-2, all methods and components for a sensor fusion approach for TraXYZ are described. Based on this information, this section presents the algorithm for sensor fusion of all sensor data provided by Sendrato's TraXYZ system. The TraXYZ system consists of two tags placed on the artist's hips. Each tag contains a UWB sensor and an IMU sensor. Hence, we have data from two UWB sensors and two IMU sensors, and the fixed relative distance between them is known. This section presents the tightly coupled sensor fusion method for UWB data and IMU data coming from two tags placed on the hips, to track an artist on stage. The goal of this method is to improve TraXYZ's tracking accuracy compared to UWB-only position tracking. Algorithm 8 on the next page combines Algorithm 4 - 7 of this chapter.

Algorithm 8 Tightly coupled EKF for UWB/IMU sensor fusion and fusion of two tags

Initialize:
  Joint state vector: $x_0 = [(x_0^{(1)})^\top \ (x_0^{(2)})^\top]^\top$
  Covariance matrix: P_0
loop
  $t \leftarrow t + 1$
  if $y_{a,t}^{(1)},\ y_{\omega,t}^{(1)}$ **then** ▷ IMU measurements
    $\hat{x}_t^{*(1)} \leftarrow f(\hat{x}_{t-1}^{(1)},\ y_{a,t}^{(1)},\ y_{\omega,t}^{(1)},\ e_{a,t}^{(1)} = 0,\ e_{\omega,t}^{(1)} = 0)$
    $\hat{x}_t^{(2)} \leftarrow \hat{x}_{t-1}^{(2)}$
    $P_t^* \leftarrow \begin{bmatrix} F_t^{(1)} & 0 \\ 0 & I_{n_2 \times n_2} \end{bmatrix} P_{t-1} \begin{bmatrix} F_t^{(1)} & 0 \\ 0 & I_{n_2 \times n_2} \end{bmatrix}^\top + \begin{bmatrix} G_t^{(1)} & 0 \\ 0 & 0 \end{bmatrix} \begin{bmatrix} Q_{t-1}^{(1)} & 0 \\ 0 & 0 \end{bmatrix} \begin{bmatrix} G_t^{(1)} & 0 \\ 0 & 0 \end{bmatrix}^\top$
    $\hat{x}_t^{(1)} \leftarrow \hat{x}_t^{*(1)}$
    $P_t \leftarrow P_t^*$
  else
    $\hat{x}_t^{*(1)} \leftarrow \hat{x}_{t-1}^{(1)}$
    $P_t^* \leftarrow P_{t-1}$
  end if
  if $y_{a,t}^{(2)},\ y_{\omega,t}^{(2)}$ **then** ▷ IMU measurements
    $\hat{x}_t^{(1)} \leftarrow \hat{x}_t^{*(1)}$
    $\hat{x}_t^{(2)} \leftarrow f(\hat{x}_{t-1}^{(2)},\ y_{a,t}^{(2)},\ y_{\omega,t}^{(2)},\ e_{a,t}^{(2)} = 0,\ e_{\omega,t}^{(2)} = 0)$
    $P_t \leftarrow \begin{bmatrix} I_{n_1 \times n_1} & 0 \\ 0 & F_t^{(2)} \end{bmatrix} P_t^* \begin{bmatrix} I_{n_1 \times n_1} & 0 \\ 0 & F_t^{(2)} \end{bmatrix}^\top + \begin{bmatrix} 0 & 0 \\ 0 & G_t^{(2)} \end{bmatrix} \begin{bmatrix} 0 & 0 \\ 0 & Q_{t-1}^{(2)} \end{bmatrix} \begin{bmatrix} 0 & 0 \\ 0 & G_t^{(2)} \end{bmatrix}^\top$
  end if
  if $T(z_{a,n}^{(1)},\ z_{\omega,n}^{(1)}) < \text{Thr}$ or $T(z_{a,n}^{(2)},\ z_{\omega,n}^{(2)}) < \text{Thr}$ **then** ▷ ZUPT detector
    $K_t \leftarrow P_t (H_t^Z)^\top \left(H_t^Z P_t (H_t^Z)^\top + R_t^Z \right)^{-1}$
    $\hat{x}_t \leftarrow \hat{x}_t - K_t H_t^Z \hat{x}_t$
    $P_t \leftarrow (I - K_t H_t^Z) P_t$
  end if
  if $y_{d,t}^{(1)}$ or $y_{d,t}^{(2)}$ **then** ▷ UWB measurements
    $S_t \leftarrow H_t^{\text{UWB}} P_t (H_t^{\text{UWB}})^\top + R_t^{\text{UWB}}$
    $CI \leftarrow c\sqrt{diag(S_t)}$
    $y_{d,t} \leftarrow \left(y_{d,t}^i |\ y_{d,t}^i - \hat{y}_{d,t}^i \in [-(CI)_i, (CI)_i] \right)$ ▷ NLOS mitigation
    $H_t^{\text{UWB}},\ R_t^{\text{UWB}} \leftarrow \left[(H_t^{\text{UWB}})_i,\ (R_t^{\text{UWB}})_i |\ y_{d,t}^i - \hat{y}_{d,t}^i \in [-(CI)_i, (CI)_i] \right]$
    $K_t \leftarrow P_t \begin{bmatrix} H_t^{\text{UWB}} \\ H_t^L \end{bmatrix}^\top \left(\begin{bmatrix} H_t^{\text{UWB}} \\ H_t^L \end{bmatrix} P_t \begin{bmatrix} H_t^{\text{UWB}} \\ H_t^L \end{bmatrix}^\top + \begin{bmatrix} R_t^{\text{UWB}} & 0 \\ 0 & R_t^L \end{bmatrix} \right)^{-1}$ ▷ Include γ
    $\hat{x}_t \leftarrow \hat{x}_t + K_t \left(\begin{bmatrix} y_{d,t} \\ \gamma \end{bmatrix} - \begin{bmatrix} H_t^{\text{UWB}} \\ H_t^L \end{bmatrix} \hat{x}_t \right)$
    $P_t \leftarrow \left(I - K_t \begin{bmatrix} H_t^{\text{UWB}} \\ H_t^L \end{bmatrix} \right) P_t$
  else
    $K_t \leftarrow P_t (H_t^L)^\top \left(H_t^L P_t (H_t^L)^\top + R_t^L \right)^{-1}$
    $\hat{x}_t \leftarrow \hat{x}_t + K_t (\gamma - H_t^L \hat{x}_t)$ ▷ Relative distance correction
    $P_t \leftarrow (I - K_t H_t^L) P_t$
  end if
end loop

Chapter 4

Results

This chapter starts with the experiment conducted to acquire datasets for testing the effectiveness of the method discussed in the previous chapter. The following sections discuss the results of applying Algorithm 8 to this dataset. The goal is to evaluate the effects of including the IMU sensor in the position estimation algorithm and the effects of joining the two tags, therefore finding answers to the research's two subquestions. From these results, it can be concluded what the potential is of the methods explained in Chapter 3 and in what situations the methods could be beneficial. As a baseline, only UWB sensors are used to estimate position. First by using only the UWB measurements in a Non-Linear Least Squares (NLS) algorithm. Second, by using the UWB measurements in an EKF that uses a Constant Velocity Model (CVM) model in the time update step. The results are shown in Section 4-2. The next section, Section 4-3, then compares the results of the UWB/IMU fusion to this baseline. It also discusses the effects of IMU bias state estimation, implementation of ZUPTs, and implementation of NLOS detection and mitigation on further improving the UWB/IMU fusion EKF. The impact of joining the two tags is discussed in Section 4-4.

4-1 Experiments

To test Algorithm 8, data has been acquired from TraXYZ in a way the true trajectory is known. Therefore, a simplified trajectory is setup for a potential artist in a theatre show. The two tags including both an UWB and IMU sensor are attached to the hips. The measurements are used as input in the models in Eq. (2-4) and Eq. (2-1) to be used in the UWB/IMU EKF for estimating the trajectory. The goal of the experiments is to analyze the potential of the methods described in previous chapter for accurately estimating the trajectory.

Figure 4-1 shows the walked trajectory during the experiment. The person walks on the sides and one diagonal of a 3m $\times$ 3m square. At the start and end, the person is stationary for approximately 30 seconds. The red crosses indicate stationary points during the walking route. Stationary point 1 is at 3m from the starting point. Points 2-4 are exactly at the middle of the sides, at 1.5m. What happens at each of these points is the following:

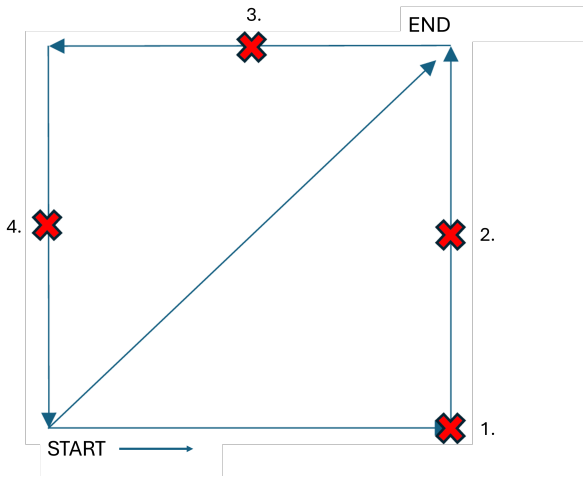

Figure 4-1: True trajectory of the experiment. The sides of the square are 3m. The stationary points are indicated with red crosses. At the start and end the person was stationary for ±30 seconds.

- Point 1: First stand still for 5 seconds, then turn left.
- Point 2: Stand still for 5 seconds, then continue walking in the same direction.
- Point 3: First turn 90° to face the "audience" (the bottom in Figure 4-1). Then stand still for 5 seconds. Then turn back 90° to continue walking the trajectory.
- Point 4: Stay at this spot for 5 seconds while changing the weight on each leg a bit. This causes a bit of hip movement on the spot.

The experiment tries to include realistic movements of a person. During the experiment the TraXYZ system is used. The anchor placement is shown in Figure 4-2. These coordinates are calculated by the calibration software in TraXYZ. The anchors are calibrated with the height of an office table (0.70m) as ground level. Compared to the real-life anchor setup, it can be concluded that these positions are not entirely accurate, particularly in the z-coordinate. That is because the anchor setup in real-life gives an idea of the anchor positions relative to each other and of the height of the anchors. These factors do not entirely match the relative positions and heights provided by the calibration software. However, due to limitations of the available UWB setup in practice, better UWB calibration was not feasible in this case. The TraXYZ tags are taped to the person's belt at the sides of the hips. The distance between the two tags is measured to be 0.27m.

The exact type of IMU sensor incorporated in TraXYZ is unknown, but presumably an LSM9DS1. TraXYZ obtains IMU measurements at a sampling frequency of approximately 120Hz. Every 6th IMU measurement is accompanied by UWB ranging measurements. As a result, the algorithm iterates through the IMU data timestamps, and every 6 iterations, it updates the state estimate using the UWB data. At times, one of the sensors may fail to provide data.

As an auxiliary experiment, a different type of IMU sensor is used in addition to the IMUs integrated in TraXYZ. These types of IMUs are the Xsens MTi-100-2A8G4 for Tag1 and the Xsens MTi-300-2A8G4 for Tag2, and are rigidly taped to the TraXYZ tags for the experiment. The first has a sampling frequency of 200Hz and the second 400Hz. Both have a bias stability of 10°/h and a noise density of $0.01°/s/\sqrt{Hz}$, where in this case Hz stands for the bandwidth of 415Hz. The same algorithm is applied to both the TraXYZ IMU data and the Xsens IMU data, in combination with the TraXYZ UWB data. When significant differences in estimation accuracy between the two IMU sensor types are found, replacing the TraXYZ IMU sensor with the Xsens IMU sensor can be recommended on top of the main research findings.

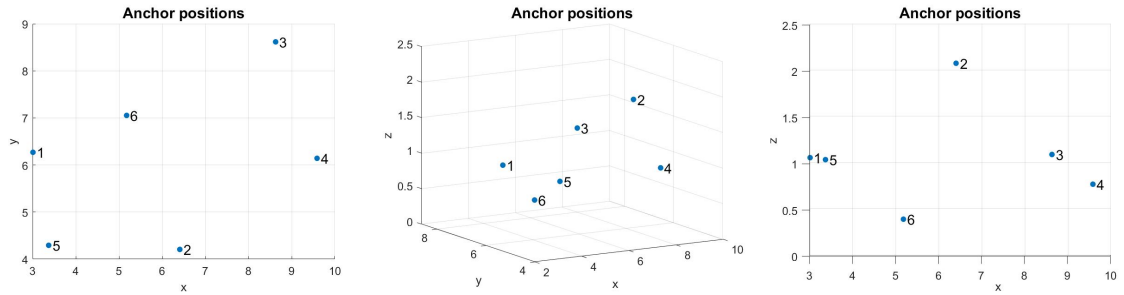

(a) Anchors xy-plane **(b)** Anchors 3D **(c)** Anchors z-coordinate

Figure 4-2: UWB anchor positions. An office table not included in the picture is used as ground level. Therefore the z-coordinate is +70cm in real life.

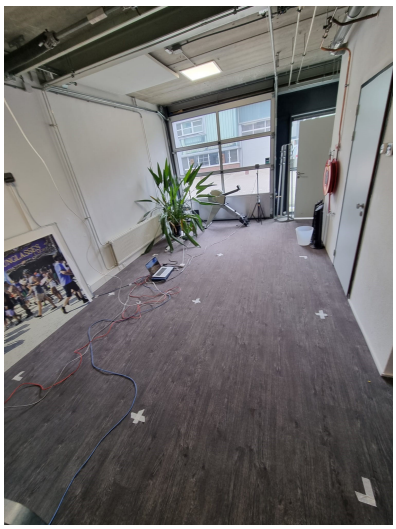

Figure 4-3: The experiment setup. The trajectory is taped on the floor.

4-2 Baseline: no IMU

As a baseline for this research, position estimation results are generated with UWB data only. That is, using the UWB data in the Non-Linear Least Squares (NLS) algorithm of Eq. (2-9). Additionally, the UWB data is used in the measurement update of an EKF, where the CVM is used in the time update. This gives some correction to the UWB measurements and therefore smooths the estimated trajectory. This method is described in Algorithm 1.

4-2-1 Non-Linear Least Squares (NLS)

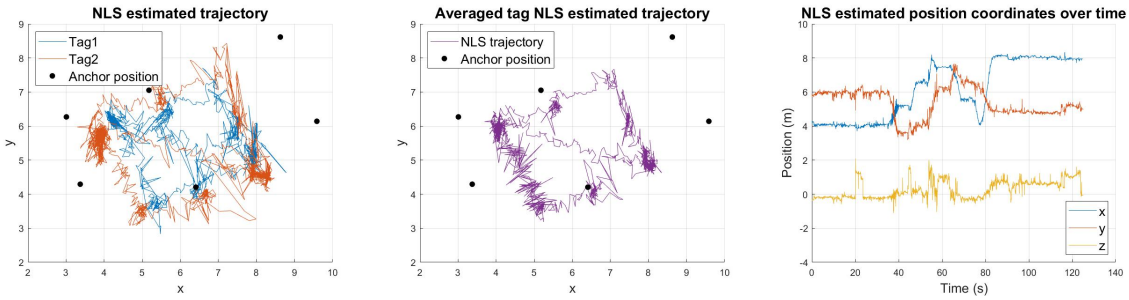

(a) Trajectory Tag1 and Tag2.

(b) Trajectory averaged tags.

(c) Coordinates averaged tags.

Figure 4-4: Position coordinates estimated with UWB measurements and the NLS algorithm in Eq. (2-9).

First, a NLS algorithm is used to find the position estimates that best fit the UWB distance measurements. The MATLAB function "lsqnonlin" along with Eq. (2-9) is used for this estimation. The initial conditions are set to $x_0^{(1)} = (4.07,\ 5.9,\ 0.3)^\top$ and $x_0^{(2)} = (3.85,\ 5.74,\ 0.3)^\top$ for Tag1 and Tag2, respectively. This is an approximation for timestep 0, based on the real-life distance to the position of anchor 1. That is because it is known the person started close to anchor 1, therefore the position coordinates of anchor 1 gave an approximate indication of the initial position of the person. Additionally, the initial conditions are chosen such that the Euclidean norm of the difference of the two vectors is approximately 0.27m; the true distance between the two tags. The anchors were calibrated with the height of the table (0.70m) as ground level. Therefore, the initial z-coordinate is set to 0.3m, which is the hips' height minus the table's height. These initial conditions are used throughout this experiment.

Figure 4-4 shows the tag's trajectory and coordinates over time, together with the anchor positions. For the averaged position estimates, the average of the two position estimates is taken. At time instances where one of the tags has no measurements, the estimate of the other tag is used solely. This happens numerous times at the left side of the trajectory in Figure 4-4b. The stationary points in the trajectory can be recognized clearly in the x-coordinate of Figure 4-4c, at the beginning and ending and the four horizontal pieces in the line.

Figure 4-4b roughly agrees with the true walked trajectory in Figure 4-1. The figures clearly show NLOS problems, as the error of each tag is visibly large. Furthermore, it is noticeable

that the estimates are unsteady at the stationary points in the trajectory. The z-coordinate estimates are not constant. This is as expected since UWB systems typically have a lower accuracy when estimating height [48]. The bottom part of the trajectory seems to go through the wall to which the anchor was attached. This could be due to the inaccurate anchor positions in Figure 4-2 provided by the calibration software.

4-2-2 EKF with Constant Velocity Model (CVM)

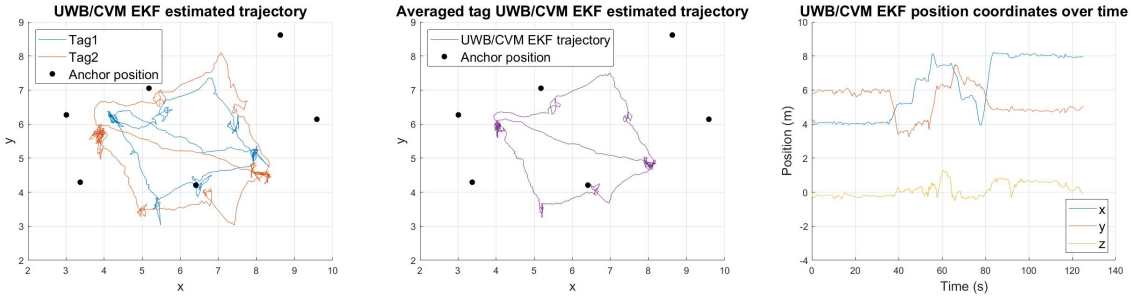

(a) Trajectory Tag1 and Tag2.

(b) Trajectory averaged tags.

(c) Coordinates averaged tags.

Figure 4-5: Position coordinates estimated with UWB measurements and an EKF with CVM.

UWB/CVM EKF parameters	
x_0	$(4.07,\ 5.9,\ 0.3,\ 0,\ 0,\ 0,\ 3.85,\ 5.74,\ 0.3,\ 0,\ 0,\ 0)^\top$
P_0^p	$0.2 \cdot I_{3\times 3}$
P_0^v	$0.05 \cdot I_{3\times 3}$
Q_t^p	$I_{3\times 3}$
Q_t^v	$I_{3\times 3}$
R_t^{UWB}	$0.25 \cdot I_{\#y_{d,t}\times \#y_{d,t}}$

Table 4-1: Parameters used for UWB/CVM EKF position estimation.

To improve the results in previous section without integrating IMU data, a Constant Velocity Model (CVM) is used in an EKF to find the position that corresponds best to the prediction from the CVM and the UWB measurements. The algorithm is described in Algorithm 1. Table 4-1 shows the parameters used for this EKF. P_0 is an approximation of the initial variance based on an approximation of the uncertainty of the initial condition. In this case, the initial position's variance is guessed to be 0.2 m^2 and the initial velocity's variance to be 0.05 m^2/s^2. R_t^{UWB} is roughly based on the variance of the UWB measurements taken during the first 30 seconds where the person was stationary. This value was then slightly increased to account for inaccuracies in the anchor positions, giving the UWB measurements more uncertainty. It was observed that increasing or decreasing R_t^{UWB} with a factor 10 resulted in minimal differences in smoothness of the outcome. Q_t is tuned until a balance is found between the trajectory's smoothness and any delays in movements. For example, when decreasing Q_t with a factor 10, a slight delay in turning the upper right corner was observed. Note that Q_t and R_t are

set constant for all t.

The estimates are smoother compared to the NLS results in previous section. The averaged trajectory in Figure 4-5b is approximately 3m$\times$ 3m with an error of circa 10 cm based on the distance between arbitrarily selected points on the corners of the estimated trajectory. NLOS errors are still present in this estimation. The "dip" in Tag1's trajectory at $\pm(5, 5.9)$ in Figure 4-5a is expected from the result in Figure 4-4a, where the UWB measurements at that spot led to erroneous estimates. A second NLOS example can be observed in Tag2's trajectory at $\pm(7.4, 3.1)$. This can be explained by the person walking close to the wall to which that particular anchor was attached. That anchor is therefore unable to accurately capture the distance to Tag2, while the other anchors experience NLOS by the person's body. On the other hand, the trajectory of Tag1 is estimated more accurately in that area, because most anchors do not experience any NLOS by the person's body. This raises the hypothesis that Tag1 may be able to correct for Tag2 when the tags are joint by a fixed distance constraint. Section 4-4 will further delve into that. Averaging the trajectories of Tag1 and Tag2 (Figure 4-5b) also partly compensates for NLOS errors, as the peaks at $\pm(7.4, 3.1)$ and the upper right corner reduced.

Subsection 3-1-4 explained methods for detecting and mitigating NLOS errors in the UWB data with an EKF. The methods intuitively reject UWB measurements $y_{d,t}$ that differ too much from the distance $\hat{y}_{d,t}$ predicted by the CVM. The results are shown and compared in Figure 4-6. The constant threshold on the absolute value of the residual in Eq. (2-11) is set to 1m. The confidence interval in Eq. (3-15) uses a 90% confidence interval with critical value $c = 1.645$ and $R_t^{\text{UWB}} = 0.25$. It can be argued that after the NLOS mitigation, R_t^{UWB} in the UWB measurement update can be decreased due to increased certainty in the remaining UWB measurements. However, it was observed that the differences in results were negligible.

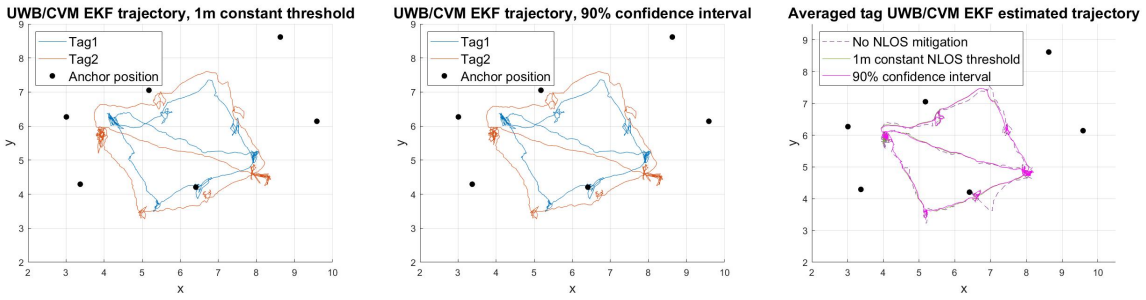

(a) Trajectory Tag1 and Tag2, 1m constant NLOS threshold.

(b) Trajectory Tag1 and Tag2, 90% confidence interval.

(c) Trajectory averaged tags.

Figure 4-6: Position coordinates estimated with UWB measurements and an EKF with CVM. Additionally, the UWB measurement outliers are rejected with the methods from Subsection 2-2-1: a constant threshold on the residual and using a 90% confidence interval on the measurements.

The NLOS issues observed before are reduced. For example, Figure 4-6c shows that the peak at $\pm(7.4, 3.1)$ disappeared. The figure additionally indicates that the 1m constant threshold

and the 90% confidence interval produced nearly identical results. The 90% confidence interval method is less arbitrary in establishing a restriction for the measurements, whereas the constant threshold can give a better understanding of how much the CVM prediction differs from the UWB measurement. In general, increasing the confidence interval percentage leads to results similar to Figure 4-5. A final observation is that the z-coordinate did not improve compared to the case without NLOS mitigation. Since the EKF with CVM already provides more accurate results than the NLS method, the UWB/CVM EKF will now serve as the baseline to evaluate whether the IMU sensor can further improve results.

4-3 UWB/IMU fusion

This section evaluates the UWB/IMU sensor fusion methods discussed in Section 3-1. The section starts with the fusion of the data without bias correction, Zero Velocity Updates (ZUPTs) and Non-Line-of-Sight (NLOS) mitigation. Subsequently, each of these elements is incorporated into the EKF and in some cases combined. The effects of each of these components are analyzed.

4-3-1 UWB/IMU fusion

As a starting point, the raw UWB and IMU data are inserted into the standard EKF of Algorithm 4. Hence no bias correction, ZUPT implementation, and NLOS mitigation are applied. The results are compared to the UWB-only results in previous section.

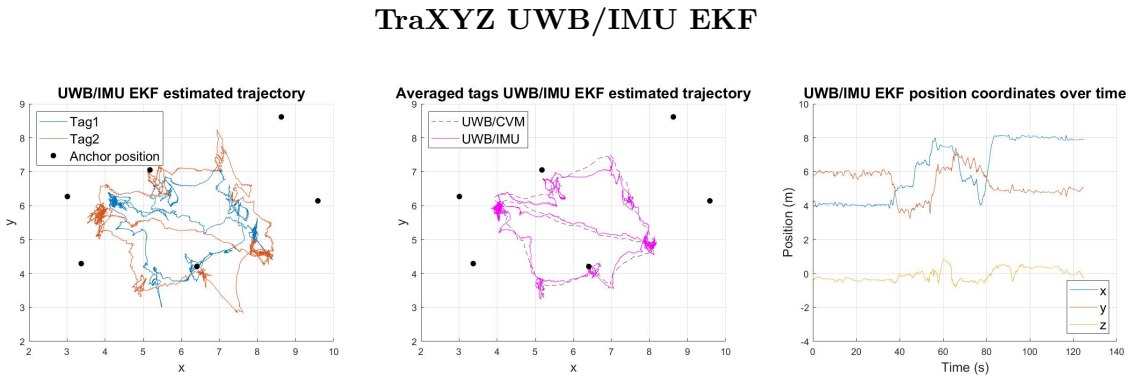

(a) Trajectory Tag1 and Tag2.

(b) Trajectory averaged tags.

(c) Coordinates averaged tags.

Figure 4-7: Position coordinates estimated with UWB measurements and an EKF with IMU model in the time update. TraXYZ's IMU measurements are used. No IMU bias is subtracted from the measurements. No NLOS mitigation.

The initial orientation is calculated using the first couple IMU data points and Eq. (3-5)-Eq. (3-8) [13]. Subsection 3-1-1 discussed that this method mainly determines initial inclination due to lack of magnetometer measurements. The heading will be corrected once UWB measurements are available. R_t^{UWB} equals the UWB measurement covariance in the UWB/CVM case. The process noise Q_t is tuned until a balance is achieved between certainty in

TraXYZ UWB/IMU EKF parameters	
x_0	$(4.07,\ 5.9,\ 0.3,\ 0,\ 0,\ 0,\ 0.62,\ -0.05,\ -0.78,\ 0.06,\ \ldots$ $3.85,\ 5.74,\ 0.3,\ 0,\ 0,\ 0,\ -0.63,\ -0.02,\ 0.77,\ 0.03)^\top$
P_0^p	$0.2 \cdot I_{3\times3}$
P_0^v	$0.05 \cdot 10^{-4} \cdot I_{3\times3}$
P_0^q	$0.3 \cdot I_{3\times3}$
$Q_{p,t}^{(m)}$, $Q_{v,t}^{(m)}$	$0.6 \cdot I_{3\times3}$
$Q_{\omega,t}^{(m)}$	$0.6 \cdot I_{3\times3}$
R_t^{UWB}	$0.25 \cdot I_{\#y_{d,t}\times\#y_{d,t}}$

Table 4-2: Parameters used for UWB/IMU EKF position estimates using TraXYZ's IMU sensors. $m = 1, 2$ for Tag1, Tag2, respectively.

UWB measurements and IMU predictions. In general, the EKF is tuned with the covariance matrices P_0, Q_t, and R_t. The initial covariance P_0 captures the uncertainty of the initial state x_0. The process noise covariance matrix Q_t takes into account the uncertainty of the dynamic IMU model as well as the IMU measurements that are used as input. The measurement noise covariance matrix R_t accounts for the uncertainty in the UWB measurements. Smaller Q_t led in this experiment to more inaccurate results. On the other hand, when increasing Q_t it can be argued that the IMU measurements do not significantly contribute to the results at all.

The true trajectory is recognizable from these estimated positions. The resulting trajectory is improved compared to the NLS case in Figure 4-4, indicating that the IMU measurements can compensate for UWB errors. However, the trajectory is less smooth than the CVM case in Figure 4-5. This can be explained by the measurement input in the IMU model Eq. (2-4). These measurements contain bias that is not eliminated yet in this algorithm and is accumulating over time. The UWB measurements are not sufficiently accurate to correct for these IMU errors. The expectation is that a ZUPT and bias correction will mitigate these errors.

The same is done with the Xsens sensors. Applying an EKF without bias correction, ZUPT implementation and NLOS mitigation provided in Algorithm 4 leads to the results in Figure 4-8. The resulting trajectory is smoother compared to Figure 4-7. The process noise Q_t could afford a lower value compared to the TraXYZ case, indicating more certainty in the Xsens measurements. Moreover, the process noise is almost ten times smaller than in the CVM case, while generating similar results. This shows that the Xsens IMU sensors contain less bias and noise and consequently provide more accurate results. It can also be concluded that the Xsens IMU sensor can improve UWB-only position estimation with NLS.

4-3-2 Bias estimation

To account for the bias present in the IMU measurements, the methods in Subsection 3-1-2 are applied and evaluated in this subsection. The IMU bias $\delta_{a,t}$ and $\delta_{\omega,t}$ are included in the state and estimated by the EKF. For each timestep, the estimated bias is subtracted from the IMU measurements. The resulting trajectory is shown in Figure 4-9. The estimated bias over

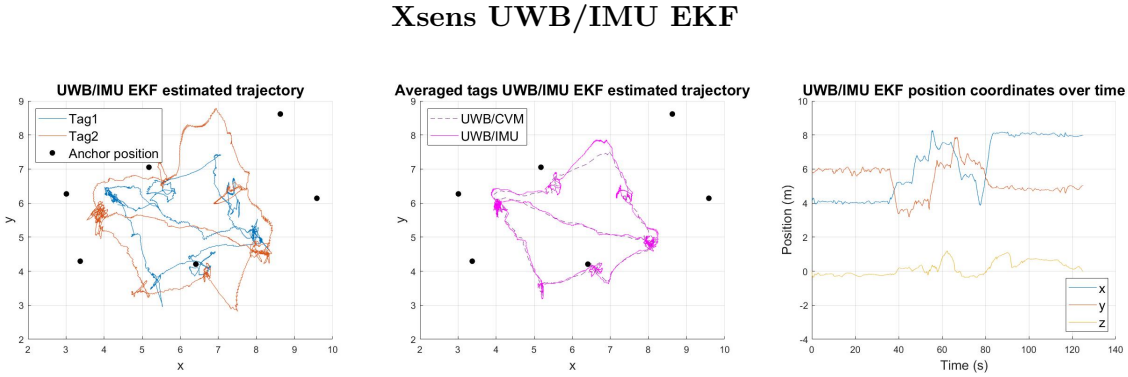

(a) Trajectory Tag1 and Tag2.

(b) Trajectory averaged tags.

(c) Coordinates averaged tags.

Figure 4-8: Position coordinates estimated with UWB measurements and an EKF with IMU model in the time update. Xsens' IMU measurements are used. No IMU bias is subtracted from the measurements. No NLOS mitigation.

Xsens UWB/IMU EKF parameters	
x_0	$(4.07,\ 5.9,\ 0.3,\ 0,\ 0,\ 0,\ -0.76,\ 0.06,\ 0.64,\ -0.05,\ \ldots$ $3.85,\ 5.74,\ 0.3,\ 0,\ 0,\ 0,\ 0.76,\ 0.02,\ -0.65,\ -0.02)^\top$
P_0^p	$0.2 \cdot I_{3\times3}$
P_0^v	$0.05 \cdot 10^{-4} \cdot I_{3\times3}$
P_0^q	$0.3 \cdot I_{3\times3}$
$Q_{p,t}^{(m)}$, $Q_{v,t}^{(m)}$	$0.2 \cdot I_{3\times3}$
$Q_{\omega,t}^{(m)}$	$0.2 \cdot I_{3\times3}$
R_t^{UWB}	$0.25 \cdot I_{\#y_{d,t}\times\#y_{d,t}}$

Table 4-3: Parameters used for UWB/IMU EKF position estimates using Xsens' IMU sensors. $m = 1, 2$ for Tag1, Tag2, respectively.

time is shown in Figure 4-10. Table 4-4 provides the bias estimation parameters. Additionally, the algorithm uses the EKF parameters from Table 4-2. The initial bias is set to zero to see if the value will converge. The initial bias state covariance $P_0^{\delta_a}$ and $P_0^{\delta_\omega}$ has to be reasonably large to ensure quick convergence at the start, hence the value 0.5 is chosen ($\approx 0.7^2$). Since the bias is expected to stay nearly constant for the duration of this experiment, the noise covariances $Q_t^{\delta_a}$, $Q_t^{\delta_\omega}$ in the random walk bias model Eq. (2-8) are set very small: 10^{-10}.

Figure 4-9 indicates that the trajectory has improved at many locations compared to Figure 4-7. For example, Tag1's trajectory shows straighter lines, mostly the first two sides (left and bottom side). Overall, the estimated trajectory starts to approach the results from the UWB/CVM EKF in Figure 4-5 and therefore comes closer to the true trajectory. Problems with the stationary points stay present. This can be due to the unstable UWB measurements at those points. It is expected that a ZUPT can solve this and can give the EKF valuable information for the bias estimation as well.

The estimated gyroscope bias in Figure 4-10 clearly converges. The estimated accelerometer bias fluctuates more than the gyroscope bias but also converges. The bias fluctuation is expected from accelerometers. A notable change in estimated bias happens at about 46s in Figure 4-10b, after the initial convergence was completed. This is exactly where the first stationary point ended and the person continued walking. During the tuning process, this more often occurred in the results after stationary points. A possible cause could be the sudden acceleration at those moments and at the same time the noisy UWB measurements or UWB outliers. Another explanation could be that including bias estimation does generally not always improve performance because position, heading, and gyroscope bias around the vertical axis are unobservable during stationary moments [49], [50], [51], [52]. The accelerometer and gyroscope cannot determine the heading, only the inclination. The magnetometer in the IMU sensor often determines heading, but this is not available in theatre situations due to magnetic disturbances. Alternatively, the position derived from UWB data can give information about the heading when combined with accelerometer and gyroscope predictions. However, at stationary points, the heading is not observable due to the lack of displacement measured by the UWB system. Therefore, when the person starts walking again, the heading becomes observable and the bias can change. This occurs mainly in the y and z direction in Figures 4-10a and 4-10b. The acceleration in the y and z directions in the sensor frame correspond to the horizontal accelerations in the navigation frame and, therefore related to heading. These sudden bias changes could lead to inaccurate results. However, in this case, it is accepted since the trajectory seems not too much affected by this. The same theory may explain why the gyroscope bias in the x direction in Figures 4-10c and 4-10d is larger than expected from the raw gyroscope measurements. The angular velocity around the x-axis in the sensor frame corresponds to the angular velocity around the z-axis (vertical axis) in the navigation frame, therefore corresponding to the yaw or heading. Since the heading is unobservable at stationary points, the gyroscope bias around the vertical axis is less accurately estimated [49], [50], [52]. Additionally, one could argue that the gyroscope bias is incorrectly estimated at the stationary point at the start without available heading information, and subsequently remaining constant due to the low value for $Q_t^{\delta_\omega}$. Values up to $Q_t^{\delta_\omega} = 10^{-4}$ are tested and it was found that the gyroscope bias around the vertical axis does not significantly reduce without the overall gyroscope bias excessively fluctuating. In general, UWB data is necessary for accurate bias estimation with an EKF, because the position information that the UWB system provides should reduce the IMU bias drift and additionally give more information about the difference between the IMU prediction and the UWB position estimate. This difference provides information for the magnitude of the IMU bias. When UWB data is erroneous, the bias estimation could be negatively affected by that.

Once the IMU bias is subtracted from the measurement input, it is expected that the certainty in the process model and measurement input increases. Therefore, one could argue that performing IMU bias correction means that the process noise covariance for the other states, $Q_{p,t}^{(i)}$, $Q_{v,t}^{(i)}$, $Q_{\omega,t}^{(i)}$, can decrease. In this experiment, it was found that decreasing Q_t for p, v, and q without changing $Q_t^{\delta_a}$ and $Q_t^{\delta_\omega}$ resulted in less accurate trajectories. Therefore the value for Q_t remained equal to Table 4-2 for these results.

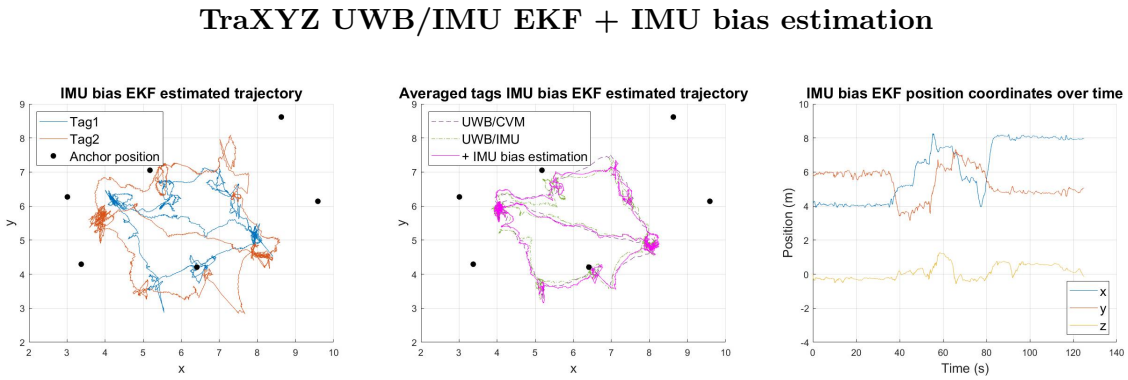

(a) Trajectory Tag1 and Tag2.

(b) Trajectory averaged tags.

(c) Coordinates averaged tags.

Figure 4-9: Position coordinates estimated with UWB measurements and an EKF with IMU model in time update. TraXYZ IMU measurements are used. Bias is estimated in the state and subtracted from the measurements in each time step. No NLOS mitigation.

Bias estimation parameters	
δ_0^a	$(0,\ 0,\ 0)^\top$
δ_0^ω	$(0,\ 0,\ 0)^\top$
$P_0^{\delta_a}$	$0.5 \cdot I_{3\times3}$
$P_0^{\delta_\omega}$	$0.5 \cdot I_{3\times3}$
$Q_t^{\delta_a}$	$10^{-10} \cdot I_{3\times3}$
$Q_t^{\delta_\omega}$	$10^{-10} \cdot I_{3\times3}$

Table 4-4: Parameters used for the bias estimation.

4-3-3 Zero Velocity Update (ZUPT)

In previous results, the stationary points remain unstable. Subsection 3-1-3 explains a method for correcting the estimates during stationary points based on IMU data. Once the ZUPT detector in Eq. (3-10) detects a stationary point based on IMU data, the velocity is corrected to 0. The applied ZUPT method is summarized in Algorithm 5. The hypothesis is that these intermittent corrections can prevent part of the IMU integration drift as well.

The algorithm is tuned with the ZUPT parameters of Table 4-5. These are found by adjusting the number of measurements N that the ZUPT detector each time considers, as well as the detection thresholds for Tag1 and Tag2, until the true stationary points are captured. The threshold Thr can be determined by calculating Eq. (3-11) during a known stationary point, for example, the beginning or end of the trajectory. The noise variances σ_a^2 and σ_ω^2 are based on the values for Q_t in Table 4-2. For the SHOD detector, only the ratio $\sigma_a^2/\sigma_\omega^2$ determines the detector's performance [47]. Besides the ZUPT parameters in Table 4-5, the EKF parameters in Table 4-2 are applied. However, it was found that the process noise covariance Q_t could be lowered from 0.6 to 0.4 when applying a ZUPT, presumably due to the ZUPT reducing the accumulating process errors. Hence, Figure 4-12 and 4-11 show the results when $Q_t = 0.4$ for p, v, and q.

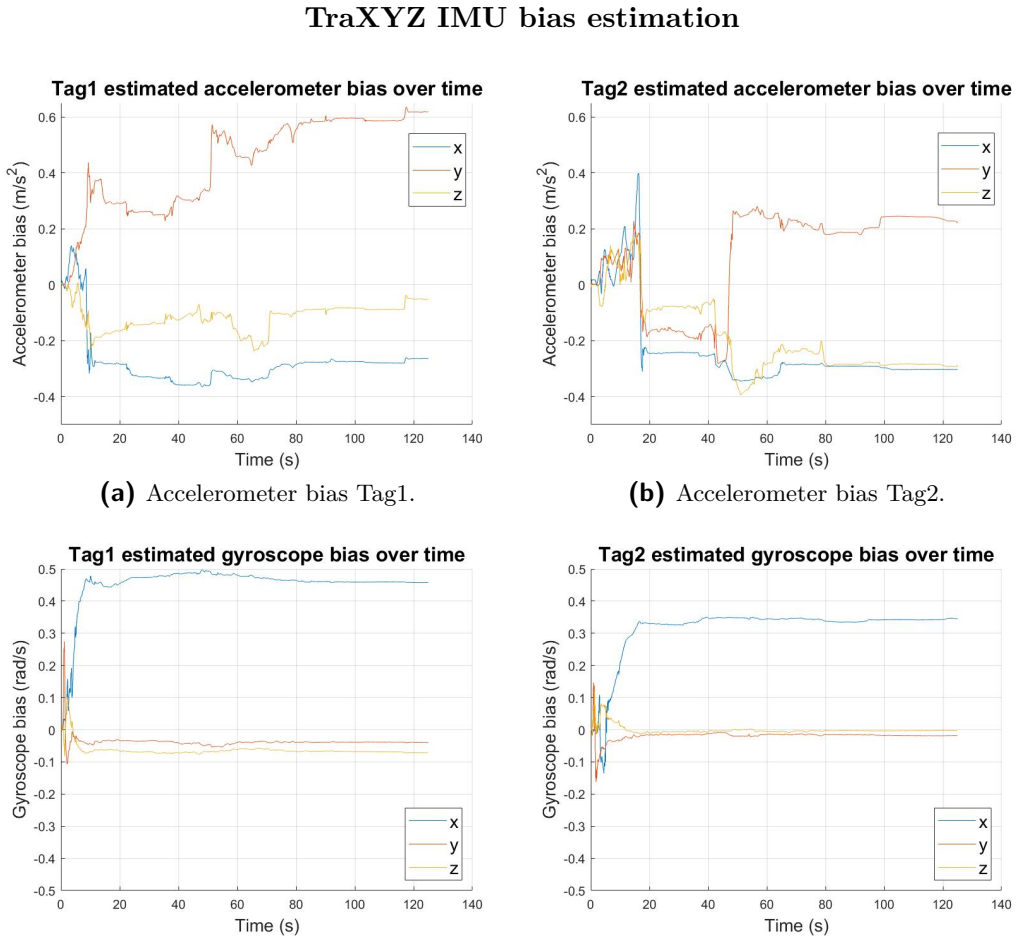

(a) Accelerometer bias Tag1.

(b) Accelerometer bias Tag2.

(c) Gyroscope bias Tag1.

(d) Gyroscope bias Tag2.

Figure 4-10: Estimated bias over time.

Figure 4-11b visualizes how the estimated position coordinates improve compared to the UWB/CVM EKF estimates. The main difference is that for the UWB/IMU EKF with ZUPTs, the stationary points are recognizable by the constant horizontal lines. Moreover, the z-coordinate remains more constant for the UWB/IMU EKF with ZUPTs. Figure 4-11a displays the estimated position coordinates over time with vertical bars indicating the start or endpoint of a stationary period. These points correspond to the time instances where the ZUPT detector continually satisfies the condition in Eq. (3-10) and where it stops meeting the condition. In between two vertical bars, the coordinates are nearly constant. Stationary point 4 in Figure 4-1, at approximately 72s in Figure 4-11, and at the upper side of the trajectory, is more difficult to capture by the IMU data. At that location, the hips moved a lot, but the person stayed in one place. This is hard to capture when the UWB data is also noisy at that point. In Figure 4-11a this can be observed by the alternating ZUPT detection and movement. Overall, the true stationary points are captured. At 56s an extra ZUPT is detected at a single time instant. Fortunately, this single detection does not affect the overall trajectory.

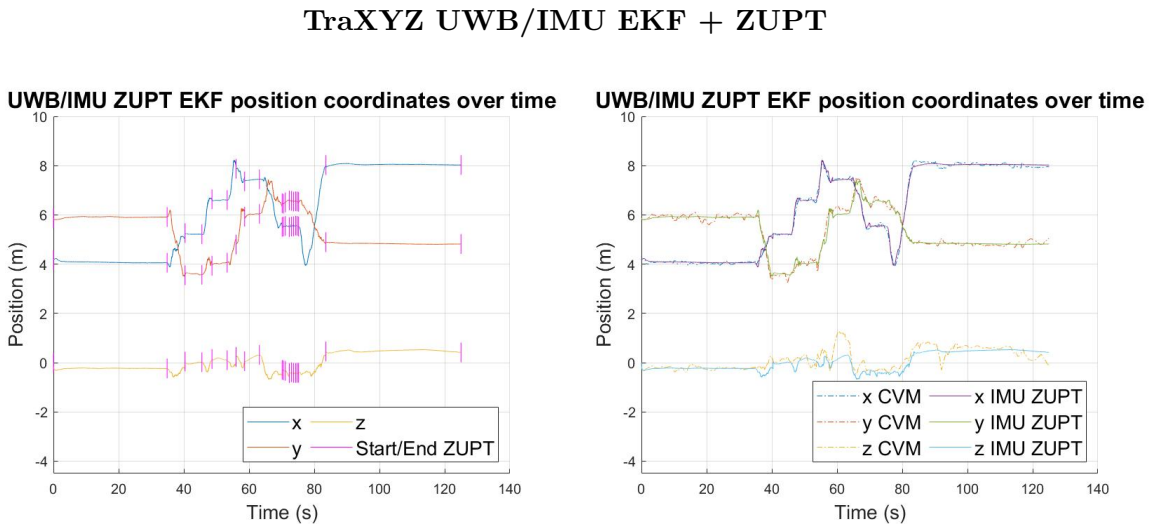

(a) Coordinates averaged tags with ZUPT detector.

(b) Coordinates averaged tags compared to UWB/CVM EKF.

Figure 4-11: Position coordinates estimated with UWB measurements and an EKF with IMU model in time update. TraXYZ IMU measurements are used. No IMU bias is subtracted from the measurements. No NLOS mitigation. A ZUPT is applied. The purple vertical bars indicate the period's start or end where the ZUPT detector detects a stationary point. The second figure compares the UWB/IMU EKF with ZUPT to the UWB/CVM EKF.

Figure 4-11b shows that the averaged trajectory approaches the true trajectory more accurately than the UWB/CVM EKF and the UWB/IMU EKF without ZUPTs. Moreover, some NLOS problems as well as the IMU integration drift reduced. However, the individual trajectories of the two tags show a couple of inaccurate bends. Presumably due to UWB outliers and the position and heading being unobservable during ZUPTs [49], [50], [51], [52]. The latter can cause errors in position and heading in the trajectory [50]. It can be concluded that the ZUPT itself works, as the true stationary points are captured and the trajectory is corrected during the stationary points. Problems can still occur before and after the ZUPT locations.

It was additionally tested to include both a ZUPT and bias estimation in the EKF of Algorithm 3. The previous subsection about bias estimation found that the accelerometer and gyroscope bias corresponding to the yaw or heading is difficult to estimate due to the unobservability of position, heading and gyroscope bias around the vertical axis during stationary points [50]. When including a ZUPT, this phenomenon was even more noticable, but the inclination also became inaccurate. The trajectory spiralled upwards, presumably due to inaccurate UWB data in the z axis (measured height) in addition to the unobservability problem. According to [49] including gyroscope bias estimation in addition to ZUPTs degrades results. Therefore, this section ends with inspecting the effects of only estimating the accelerometer bias in the state in addition to a ZUPT, while the gyroscope bias is fixed. The results are displayed in Figure 4-13. The method is achieved by adding a constant gyroscope bias statement at the end of each iteration of the EKF. Consequently, the gyroscope bias

state remains constant and is subtracted from the gyroscope measurements in each iteration. Note that in this way the gyroscope bias is not excluded from the state but is kept fixed with a constant bias update. The accelerometer bias state is unfixed and is estimated as usual. The algorithm uses the ZUPT parameters of Table 4-5. Furthermore, the bias estimation parameters of Table 4-6 are used. The process noise covariance Q_t for the position, velocity and orientation states are set back to 0.6. The value for $Q_t^{\delta_a}$ is increased to 10^{-6} to make the estimated accelerometer bias less constant. The initial value for δ_0^{ω} is set to the constant gyroscope bias value that is fixed throughout the iterations. This value is found by taking the average of the gyroscope measurements during the first 30 seconds of the trajectory. During this stationary point, it is expected that the gyroscope measurements are zero. Therefore the mean of the measurements during this time interval serves as an indication of the gyroscope bias present in the sensors. Hence, the gyroscope bias is fixed to $(0.0257\ 0.0462\ 0.0252)^\top$ for Tag1 and $(0.1143\ -0.0312\ 0.0368)^\top$ for Tag2. These calculated biases in the y and z axis are about the same as the estimated values in Figure 4-10. The results indicate that the averaged trajectory does not significantly improve compared to Figure 4-9b and 4-12b. However, Figure 4-13 shows that this method mitigates some inaccurate bends in the ZUPT results of Figure 4-12a. The trajectories approach the results of the bias estimation in Figure 4-9, while the stabilization of the stationary points is a beneficial additional result. Remaining errors can be attributed to accumulating gyroscope bias still present, as this constant value may not be entirely accurate. The estimated bias over time is shown in Figure B-1 in Appendix B, where the gyroscope bias is constant over time. The accelerometer bias in the y and z direction converge to a different value than Figure 4-10.

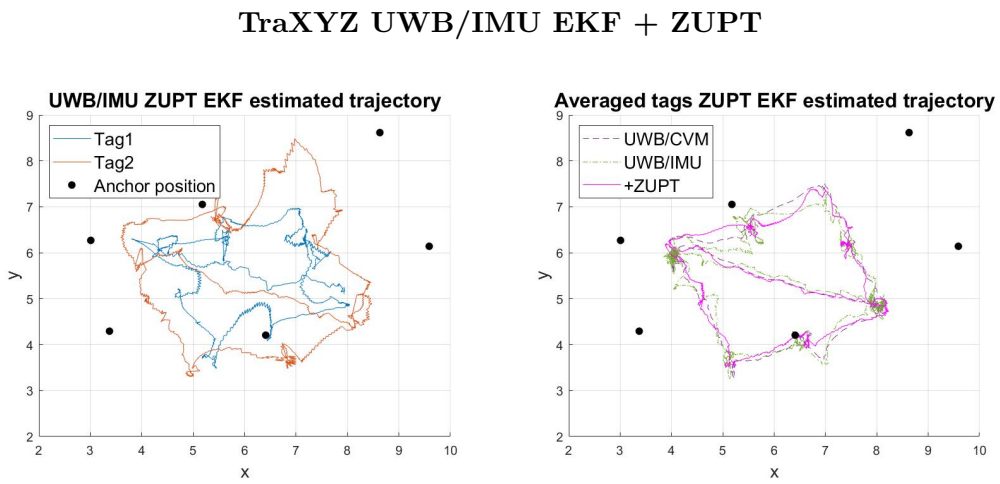

(a) Trajectory Tag1 and Tag2. **(b)** Trajectory averaged tags.

Figure 4-12: Position coordinates estimated with UWB measurements and an EKF with IMU model in time update. TraXYZ IMU measurements are used. No IMU bias is subtracted from the measurements. No NLOS mitigation. A ZUPT is applied.

TraXYZ UWB/IMU EKF + IMU bias estimation + ZUPT

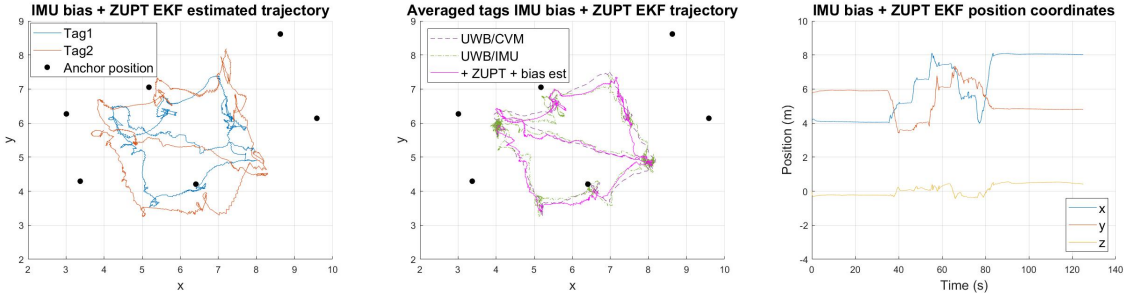

(a) Trajectory Tag1 and Tag2.

(b) Trajectory averaged tags.

(c) Trajectory averaged tags.

Figure 4-13: Position coordinates estimated with UWB measurements and an EKF with IMU model in time update. TraXYZ IMU measurements are used. No NLOS mitigation. A ZUPT is applied and only accelerometer bias is estimated and subtracted.

ZUPT parameters	
N	5
σ_a^2	0.6
σ_ω^2	0.6
$Thr^{(1)}$	0.3
$Thr^{(2)}$	0.25
R_t^{ZUPT}	10^{-7}

Table 4-5: Parameters used for the ZUPT.

Bias estimation parameters if ZUPT implementation	
$\delta_0^{a,(m)}$	$(0,\, 0,\, 0)^\top$
$\delta_0^{\omega,(1)}$	$(0.0257,\, 0.0462,\, 0.0252)^\top$
$\delta_0^{\omega,(2)}$	$(0.1143,\, 0.0312,\, 0.0368)^\top$
$P_0^{\delta_a}$	$0.5 \cdot I_{3\times3}$
$P_0^{\delta_\omega}$	$0.5 \cdot I_{3\times3}$
$Q_t^{\delta_a}$	$10^{-6} \cdot I_{3\times3}$
$Q_t^{\delta_\omega}$	$10^{-10} \cdot I_{3\times3}$

Table 4-6: Parameters used for the bias estimation when additionally a ZUPT is included. $m = 1, 2$ for Tag1 and Tag2, respectively.

4-3-4 Non-Line-of-Sight (NLOS) detection and mitigation

This subsection applies the methods for mitigating NLOS errors in the UWB data discussed in Subsection 3-1-4. The techniques are also applied and discussed in Subsection 4-2-2. In this subsection it is chosen to analyze the 90% confidence interval method for NLOS detection,

because this method is less arbitrary in establishing a restriction for the measurements than the method that uses a constant threshold on the residuals. The NLOS method applied is provided in Algorithm 6. The confidence interval method is first applied to the UWB/IMU EKF without bias estimation and ZUPT. The EKF uses the parameters in Table 4-2. The value of R_t^{UWB} in the NLOS algorithm, used for the calculation of the confidence interval in Eq. (3-15), is set to 0.4. This is higher than $R_t^{\text{UWB}} = 0.25$ that was set initially. However, it was found that when R_t^{UWB} for Eq. (3-15) was set to 0.25, the trajectory of Tag1 diverges. This happens when too many UWB measurements are rejected due to the IMU predictions drifting from the UWB distance measurements. As a consequence, the algorithm has too few UWB measurements to determine the person's heading. Including more UWB uncertainty in the confidence interval determination prevented the diverging trajectory. In the UWB measurement update, R_t^{UWB} is again 0.25. This value then indicates the uncertainty of the remaining UWB measurements. Figure 4-14 indicates that the resulting trajectory is slightly more accurate compared to Figure 4-7, for both the individual tag trajectories as the averaged trajectory.

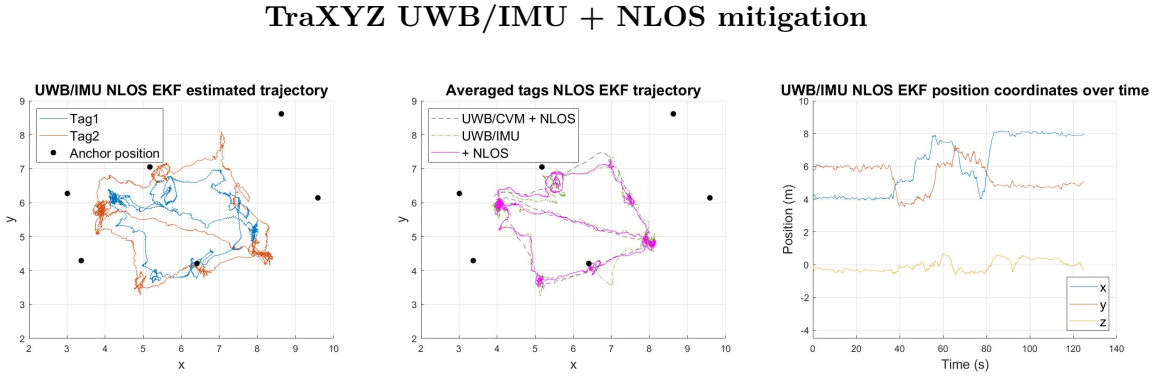

(a) Trajectory Tag1 and Tag2.

(b) Trajectory averaged tags.

(c) Coordinates averaged tags.

Figure 4-14: Position coordinates estimated with UWB measurements and an EKF with an IMU model in the time update. TraXYZ IMU measurements are used. The EKF includes NLOS detection and mitigation using a 90% confidence interval, both for the CVM and the IMU model EKF.

The NLOS mitigation with confidence interval is also applied to the EKF including IMU bias estimation and to the EKF including a ZUPT implementation, according to Algorithm 3. For the EKF with IMU bias estimation, the averaged trajectory shown in Figure 4-15b is considered more accurate than the results in Figure 4-9b. However, when inspecting Figure 4-15a, it can be concluded that Tag1 is accurate, whereas Tag2 loses accuracy in the upper side and diagonal of the trajectory, meaning the last part of the walk. This may be due to useful UWB measurements being rejected by the NLOS method, therefore losing heading information. The algorithm for the IMU bias estimation and NLOS mitigation uses the parameters in Table 4-2 and Table 4-4. The value for R_t^{UWB} used for the calculation of the confidence interval is in this case 0.25. The estimated accelerometer and gyroscope bias over time are shown in Figure B-2 in Appendix B. Mainly the accelerometer and gyroscope bias of Tag2 have increased compared to the estimated bias in Figure 4-10.

TraXYZ UWB/IMU + bias estimation + NLOS mitigation

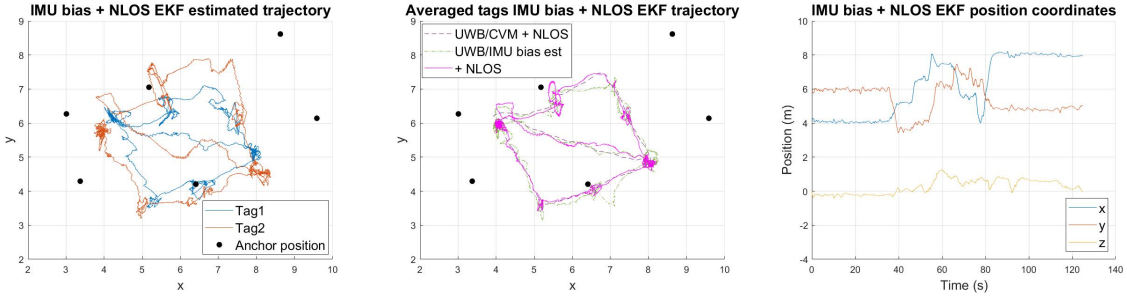

(a) Trajectory Tag1 and Tag2.

(b) Trajectory averaged tags.

(c) Coordinates averaged tags.

Figure 4-15: Position coordinates estimated with UWB measurements and an EKF with an IMU model in the time update. TraXYZ IMU measurements are used. The IMU bias is estimated in the state and corrected for. The EKF includes NLOS detection and mitigation using a 90% confidence interval, both for the CVM and the IMU model EKF.

Figure 4-16 shows the results of Algorithm 3 when the ZUPT implementation and NLOS mitigation are included. The results indicate that the trajectory does not improve accuracy compared to earlier results. The algorithm introduces some inaccurate bends in the trajectory. This was already observed in the ZUPT results without NLOS mitigation. The NLOS mitigation was not able to solve this. It can be concluded that the NLOS mitigation does not add value to the ZUPT algorithm. The algorithm that provided these figures uses the parameters in Table 4-5. Additionally the parameters in Table 4-2 are used, where Q_t for p, v, and q are in this case reduced to 0.4, similar to the previous subsection. The value for R_t^{UWB} is set to 0.4 for the confidence interval calculation and set back to 0.25 for the UWB measurement update.

TraXYZ UWB/IMU + ZUPT + NLOS mitigation

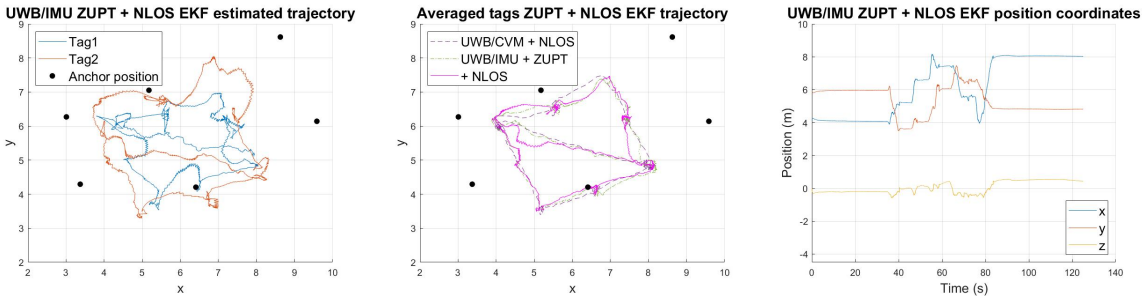

(a) Trajectory Tag1 and Tag2.

(b) Trajectory averaged tags.

(c) Coordinates averaged tags.

Figure 4-16: Position coordinates estimated with UWB measurements and an EKF with an IMU model in the time update. TraXYZ IMU measurements are used. A ZUPT is applied. The EKF includes NLOS detection and mitigation using a 90% confidence interval, both for the CVM and the IMU model EKF.

The previous subsection discussed that including bias estimation of both the accelerometer

and the gyroscope, along with a ZUPT, does not perform accurately. It is observed that adding NLOS detection and mitigation to this algorithm does not solve this. Therefore, in this final experiment, the NLOS mitigation with 90% confidence interval is added to the accelerometer bias estimation and ZUPT method used at the end of the previous subsection. For this algorithm the parameters in Table 4-5 and Table 4-6 are used along with Table 4-2. That is, the gyroscope bias remains fixed and the accelerometer bias is estimated by the EKF. For this experiment R_t^{UWB} used to calculate the confidence interval is 0.25. Figure 4-17 indicates the trajectory is almost accurate except for some bends. The inaccurate parts could partly be attributed to accumulating gyroscope bias that this EKF does not estimate. The individual trajectories are close to the true square shape.

TraXYZ UWB/IMU + bias estimation + ZUPT + NLOS mitigation

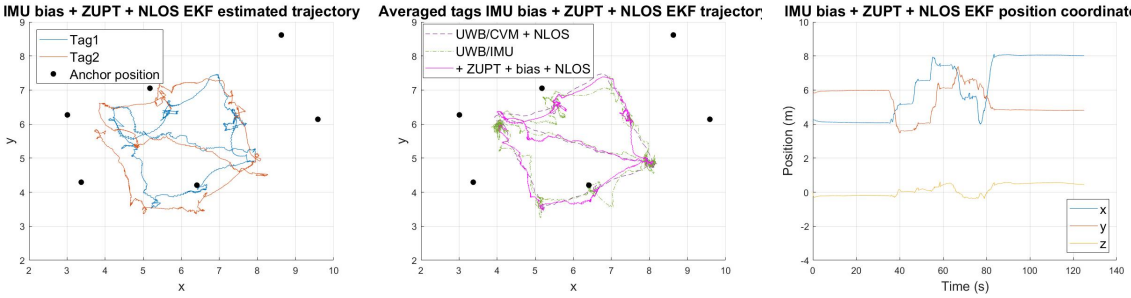

(a) Trajectory Tag1 and Tag2.

(b) Trajectory averaged tags.

(c) Coordinates averaged tags.

Figure 4-17: Position coordinates estimated with UWB measurements and an EKF with an IMU model in the time update. TraXYZ IMU measurements are used. A ZUPT is applied and accelerometer bias is estimated in the state. The EKF includes NLOS detection and mitigation using a 90% confidence interval, both for the CVM and the IMU model EKF.

4-4 Joint tags

The second subquestion of this research is about the tight coupling of the two tags on the hips, and evaluating whether the tags can correct each other's estimates to, ultimately, improve accuracy compared to loosely coupled tags. Section 3-2 discussed a method to research the effect of tightly coupled tags; augmenting the measurement equations with an equality constraint on the distance between the two tags on the hips. It is assumed that this distance is fixed and is measured to be 0.27m for the person walking the trajectory. Therefore, in this section Algorithm 7 is added to the EKF with $\gamma = 0.27$.

4-4-1 Joint tags with CVM

To start with, the effects of joint tags are evaluated for the UWB/CVM EKF. The EKF uses the same parameters as in Table 4-1. For joining the tags, the parameters $\gamma = 0.27$ and $R_t^L = 10^{-10}$ are used. The latter value represents the noise on the fixed distance measurement between the two tags.

Figure 4-5a and 4-18b show that the trajectories of the individual tags become more accurate when joining the tags. The distance between the tags indeed remains approximately 0.27m. However, Figure 4-18c shows that, in this case, the averaged trajectory is similar for the loose tags and joint tags. Figure 4-19 shows two results when the UWB/CVM EKF is tuned slightly "worse". First by decreasing the process noise covariance Q_t to 0.1, meaning the algorithm puts more certainty in the CVM model. This causes some lag when turning the upper right corner for the loose tags. Secondly, by reducing the threshold on the residuals in the NLOS detection to 0.5m. This results in too many UWB measurements being rejected by the algorithm. In both cases, the results for the loose tags averaged trajectory become less accurate, while the results for the joint tags remain nearly unaffected. For example, Figure 4-19a shows that for loose tags the algorithm introduces a delay in the upper right corner, whereas the joint tags remained on the true track. Figure 4-19b shows that for loose tags the trajectory diverges from the true trajectory when too many UWB measurements are rejected, whereas the joint tags were better resistant to this problem. These results indicate that for this experiment and a UWB/CVM EKF, the algorithm demonstrates to be less sensitive to errors caused by tuning parameters.

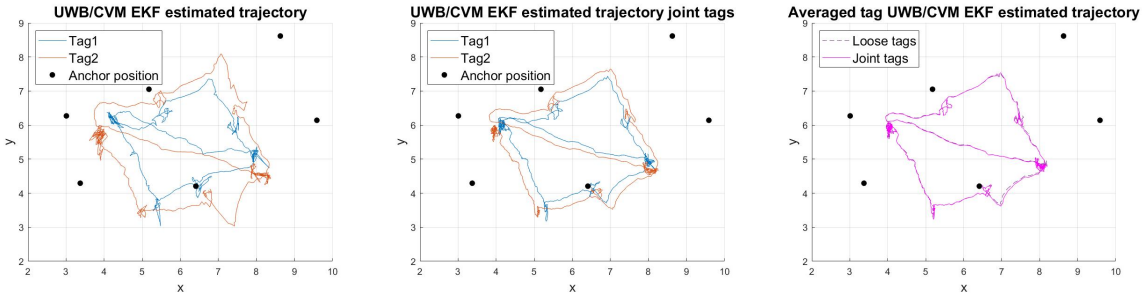

(a) Trajectory Tag1 and Tag2, loose tags.

(b) Trajectory Tag1 and Tag2, joint tags.

(c) Trajectory averaged tags.

Figure 4-18: Position coordinates estimated with UWB measurements and an EKF with CVM for loose tags and joint tags.

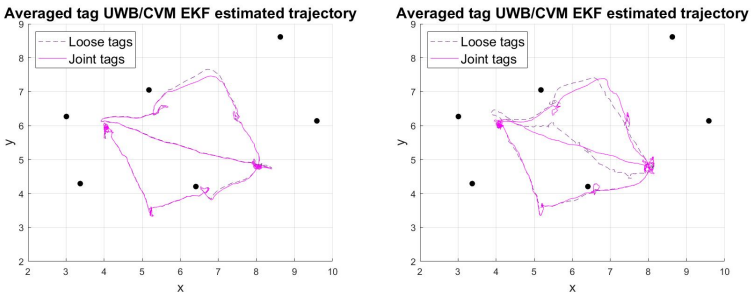

(a) Trajectory averaged tags, $Q = 0.1$.

(b) Trajectory averaged tags, $r_t^i < 0.5$m.

Figure 4-19: Position coordinates estimated with UWB measurements and an EKF with CVM for loose tags and joint tags. The EKF is tuned slightly "worse". First by decreasing Q in Table 4-1 to 0.1. Second by keeping the parameters of Table 4-1 but decreasing the threshold on the residual from 1m to 0.5m.

4-4-2 Joint tags with UWB/IMU fusion

For the UWB/IMU EKF, the tags are joined similarly. Algorithm 7 is used with the EKF parameters of Table 4-2, along with $\gamma = 0.27$. Tuning R_t^L differs from the UWB/CVM algorithm in the previous subsection. Setting $R_t^L = 10^{-10}$ means that the distance between the tags is strictly fixed, since the noise on the distance equation in Eq. (3-19) is almost zero. However, when applied to the UWB/IMU EKF, this low value for R_t^L causes the S_t matrix to be inverted in lines 2 and 6 of Algorithm 7 (general $H_t P_t H_t^\top + R_t$) to be close to singular. This happens for $R_t^L \leq 10^{-8}$ and imposes numerical problems. It is found that joining the tags works for $R_t^L = 10^{-3}$, as shown in Figure 4-20. Intuitively, this value means the distance between the tags has a freedom of approximately 3cm. Therefore, the fixed distance is less strictly enforced, but the tags are still coupled to correct each other's errors. This aligns with the goal of tracking artists on stage, where the individual tag trajectories do not need to maintain a strictly fixed distance, but the averaged tag trajectory needs to benefit from the tag's mutual corrections.

Figure 4-20b shows the individual trajectories intersect at some points. This may occur because the other updates in the EKF redirect individual trajectories in addition to the joint tag update, leading to possible intersections. The averaged trajectory in Figure 4-20c indicates that the joint trajectory is at points slightly more accurate than the averaged loose tags, for example the upper side of the square and the upper right corner. Only the right side has an inaccurate bend towards the left at $\pm(7.25, 5.75)$. Generally, it was found that the tighter the tag coupling (smaller R_t^L), the more the trajectories intersect, resulting in less smooth trajectories. For example, Figure B-3 in Appendix B shows the results for $R_t^L = 10^{-6}$. It may be that the individual estimated trajectories each exhibit too many unstable movements, causing tight coupling to result in unusual or unexpected directions. The higher the value for R_t^L, the more the trajectory approaches the loosely coupled tags. Therefore, in these cases, the averaged trajectory remains largely unchanged.

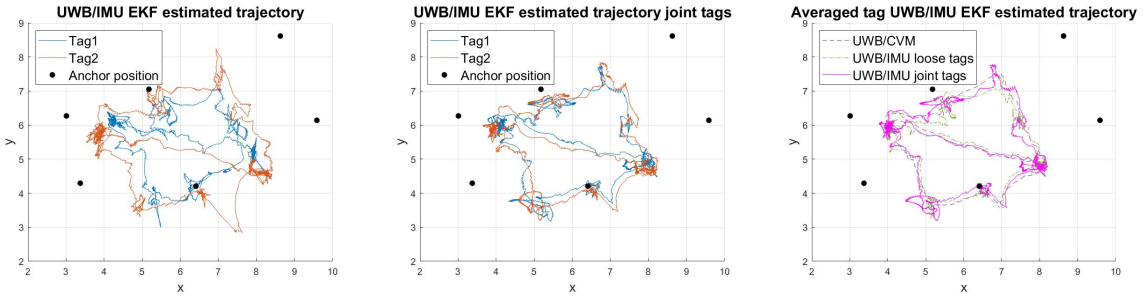

(a) Trajectory Tag1 and Tag2, loose tags.

(b) Trajectory Tag1 and Tag2, joint tags.

(c) Trajectory averaged tags.

Figure 4-20: Position coordinates estimated with UWB measurements and an EKF with an IMU model in the time update, for loose tags and joint tags. No bias correction, ZUPT, or NLOS mitigation is applied.

4-4-3 UWB/IMU fusion with joint tags, NLOS detection, ZUPT, and bias estimation

The final subsection of this chapter includes all methods discussed in Chapter 3: UWB/IMU fusion with bias estimation, ZUPT, NLOS mitigation, and joint tags. That is, Algorithm 3 is applied with all flags on. The tags are joined the same way as the previous subsection and according to the theory in Section 3-2. The parameters used remain equal to the ones used for the corresponding experiments for the loose tags in Section 4-3, with in addition a joint tag update with $\gamma = 0.27$ and $R_t^L = 10^{-3}$.

Subsection 4-3-3 and 4-3-4 discussed reasons for the reduced performance of the combination of accelerometer and gyroscope bias estimation, ZUPT, and NLOS mitigation for the loose tags. Problems observed were too large estimated gyroscope bias in the vertical axis, inclination drift, mainly of Tag1, resulting in the trajectory rising upwards, and finally, the NLOS mitigation causing some drift in the trajectory. However, joining the tags did enhance results. This can be seen in Figure 4-21. The EKF uses the ZUPT parameters of Table 4-5 and the bias estimation parameters of Table 4-4. For the calculation of the confidence interval for NLOS detection, the value for R_t^{UWB} is increased from 0.25 to 0.5. This makes sure that fewer UWB measurements are rejected in the process, which prevents the trajectory from diverging. Afterwards, $R_t^{\text{UWB}} = 0.25$ for the remaining UWB measurements in the UWB measurement update. The estimated gyroscope bias around the vertical axis remains severely large. The main difference with the loose tags is that the joint tags were able to prevent the inclination drift occurring mainly in Tag1, which can be seen in the z-coordinate of Figure 4-21b. This shows that the two tags could, to some extent, correct each other's deficiencies. The resulting averaged trajectory closely aligns with the truth, except for the notable bend on the lower right side and in the diagonal. To conclude, the application of all UWB/IMU fusion methods shows that joint tags mitigate the issues faced by loose tags. However, the estimated trajectories for both individual tags and averaged tags still exhibit certain limitations in the case of joint tags.

Apart from reducing inclination drift, joint tags can also help reduce heading drift if it occurs in one of the tags. One of the examples where this appears is the EKF with ZUPT and NLOS mitigation, where some inaccurate bends in Tag1's trajectory are reduced in the joint tag case in Figure 4-22b. For example the bends at $\pm(5, 5)$ and $\pm(6.3, 4.6)$ in Tag1's trajectory. However, it can also cause the other trajectory to show new bends because the tags are coupled. For example at $\pm(4.8, 6.8)$. These results used the EKF parameters of Table 4-2 and the ZUPT parameters from Table 4-5. Furthermore, $R_t^{\text{UWB}} = 0.4$ for the NLOS confidence interval calculation and $R_t^{\text{UWB}} = 0.25$ for the remaining UWB measurements. However, the resulting averaged trajectory did not show accurate results.

The last observed advantage of joint tags is that diverging trajectories are prevented when applying NLOS detection and mitigation. For example, for the results in Figure 4-23, the 90% confidence interval is calculated with $R_t^{\text{UWB}} = 0.3$. In this case the loose tags diverged, but the joint tags remained on track. This means that more UWB measurements could be rejected based on NLOS detection, without causing the trajectory to diverge. The loose tags needed a value $R_t^{\text{UWB}} > 0.4$ to not diverge. This phenomenon occurred more often when

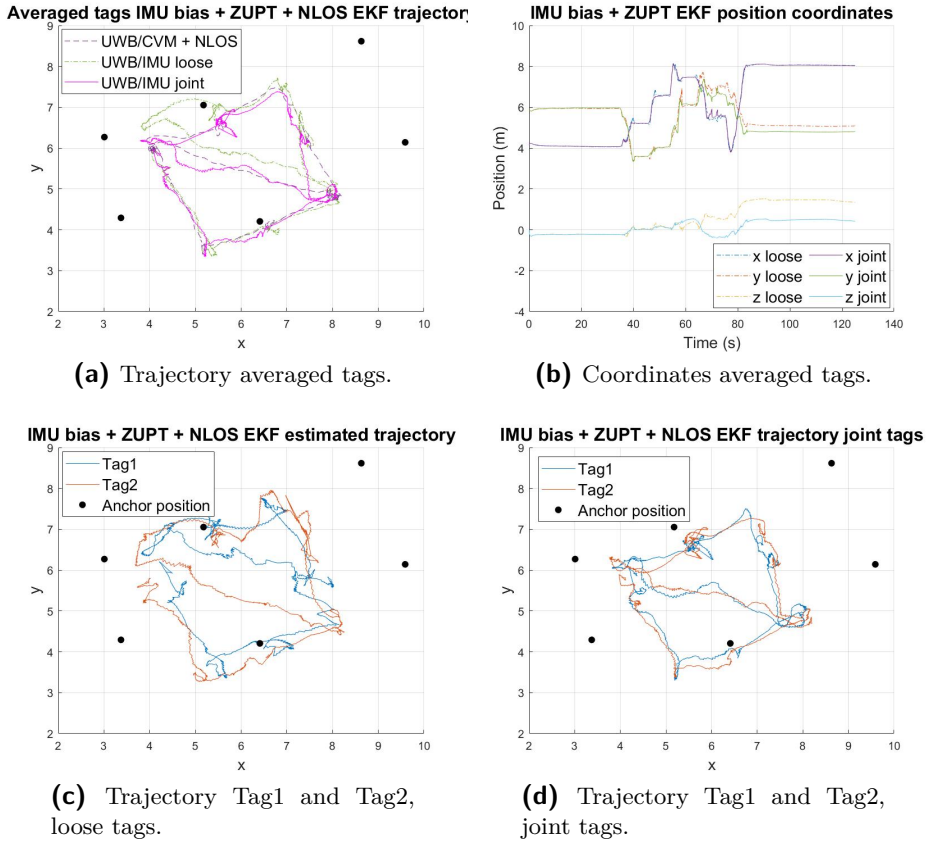

(a) Trajectory averaged tags.

(b) Coordinates averaged tags.

(c) Trajectory Tag1 and Tag2, loose tags.

(d) Trajectory Tag1 and Tag2, joint tags.

Figure 4-21: Position coordinates estimated with UWB measurements and an EKF with an IMU model in the time update, for loose tags and joint tags. Bias correction, ZUPT, and NLOS mitigation are applied.

analyzing joint tags and NLOS, also for the UWB/CVM case.

Appendix B-2 shows several auxiliary results for joint tags. Generally, it can be concluded that corrections of the individual trajectories are possible. Even though the fixed distance is not exactly preserved. That is because the value of $R_t^L = 10^{-3}$ gives some freedom to the value of the distance between the tags, together with the estimates still being propagated according to other information in the EKF. Furthermore, the joint tags' averaged trajectory often did not necessarily improve compared to the loose tags' averaged trajectory. Hence strong overall improvement due to joint tags is not observed. However it is shown that in some cases the tags can correct for each other's deficiencies, therefore showing some potential for further research on joint tags with fixed distance.

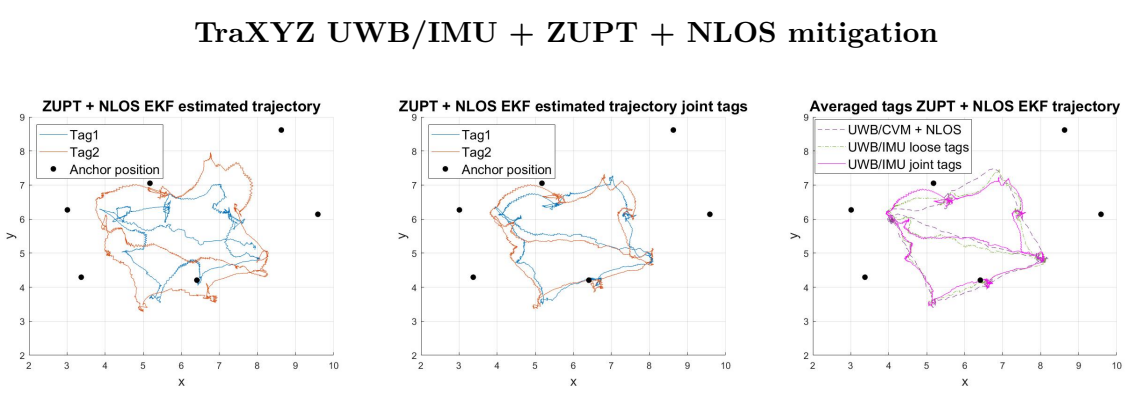

(a) Trajectory Tag1 and Tag2, loose tags.

(b) Trajectory Tag1 and Tag2, joint tags.

(c) Trajectory averaged tags.

Figure 4-22: Position coordinates estimated with UWB measurements and an EKF with an IMU model in the time update, for loose tags and joint tags. ZUPT and NLOS mitigation are applied. No bias correction included.

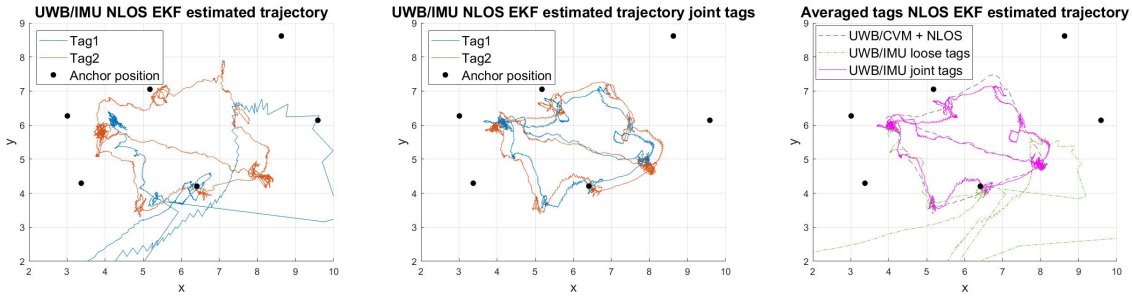

(a) Trajectory Tag1 and Tag2, loose tags.

(b) Trajectory Tag1 and Tag2, joint tags.

(c) Trajectory averaged tags.

Figure 4-23: Position coordinates estimated with UWB measurements and an EKF with an IMU model in the time update, for loose tags and joint tags. NLOS mitigation is applied. No bias correction or ZUPT included.

Chapter 5

Conclusion

5-1 Conclusion and discussion

The research studied how the sensor fusion of two coupled UWB/IMU sensors, attached to a person's hips, can be used to improve position tracking accuracy compared to using two separate UWB tags. This research question gave rise to two subquestions concerning the potential of UWB/IMU sensor fusion, and the potential of coupled tags for position tracking accuracy. This chapter aims to answer these questions and the main research question, followed by suggestions for future research and recommendations.

The first subquestion focused on the potential of UWB/IMU fusion for improving position tracking accuracy. UWB-only tracking using a Non-Linear Least Squares (NLS) algorithm showed noticeable inaccuracies and outliers. The use of an UWB/IMU Extended Kalman Filter (EKF) improved accuracy by smoothing the trajectory and correcting UWB outliers. Techniques like IMU bias correction, Zero Velocity Update (ZUPT), and Non-Line of Sight (NLOS) detection also showed potential to enhance accuracy further. While IMU bias estimation improved trajectories, challenges with heading and gyroscope bias in the vertical axis arose, presumably due to their unobservability during stationary periods or ZUPTs. Accurate UWB data is essential for bias estimation since it provides heading information without a magnetometer. A ZUPT effectively captured stationary points but struggled with hip movements and does not guarantee improved trajectory between ZUPTs. NLOS detection and mitigation helped reject UWB outliers, provided that the UWB measurement noise covariance matrix is suitable to prevent trajectory divergence. To answer this subquestion, UWB/IMU fusion can enhance position tracking accuracy but requires further refinement of these methods used for TraXYZ.

The second subquestion focused on the potential of tightly coupling the tags for position tracking accuracy. This research used two UWB/IMU sensors on the hips, enforcing a fixed distance through an equality constraint on the joint state in the EKF, therefore adding to

research on fusing multiple sensors attached to the moving object for location tracking. The fixed distance constraint was included by augmenting the EKF measurement update equations. The results indicated that joint tags could correct heading and inclination errors of individual tags, reduce divergence due to strict NLOS mitigation, and reduce the algorithm's sensitivity to tuning variability. However, the fixed distance was not consistently preserved due to increased noise covariance on the tag distance and the impact of other updates within the EKF. Nevertheless, the primary goal was mutual error correction by the tags, ensuring an averaged trajectory with increased accuracy. While joint tags can partially correct each other's trajectories, the averaged trajectory did not always improve for UWB/IMU fusion. In the case of UWB/CVM, the fixed distance can be preserved with negligible noise on the tag distance. This potentially shows that the fixed distance can be better preserved if the algorithm functions accurately. In conclusion, while joint tags have potential for improving position tracking accuracy, further research is needed for UWB/IMU sensors. This will be discussed in the next section.

The potential of UWB/IMU sensor fusion and joint tags analyzed in the two subquestions leads to answering the main research question: *"How can the sensor fusion of two coupled UWB/IMU sensors, attached to a person's hips, be used to improve position tracking accuracy compared to using two separate UWB tags?"*
The results from this experiment indicate that incorporating IMU data through an EKF can correct for UWB data impacted by NLOS and increase smoothness, as shown by the comparison with UWB-only NLS algorithm results. However, using a Constant Velocity Model (CVM) instead of IMU sensors can do this as well. This could be because the CVM is better suited for modelling the true walk in this specific experiment, which might already resemble a constant velocity walk. Since the IMU in principle provides more information, it is expected that for different walking trajectories with more bends and turns, the IMU model is preferred over the CVM. Then techniques such as IMU bias estimation, ZUPT, and NLOS detection have shown potential for further improvement of UWB/IMU fusion tracking. The observed effectiveness of tightly coupled tags lies in the ability to mutually correct individual trajectories and reduce sensitivity to tuning variability, though the averaged trajectory might not significantly improve. The UWB/CVM EKF showed that the joint tags method can function effectively.

The limitations of the tightly coupled joint UWB/IMU EKF are mainly attributed to the quality of UWB data in this experiment, which has evident inaccuracies and outliers, especially in the z-direction. While the IMU can correct some UWB errors, it also contains bias and noise that accumulate over time. Therefore, sufficiently accurate UWB data is necessary to compensate for that. The UWB data is important for heading estimation without magnetometer and for IMU bias estimation. Inaccurate UWB data is most likely the main reason for the limited performance of the developed algorithm. It was additionally found that the Xsens IMU sensor generates more accurate results than the TraXYZ sensor due to its smaller inherent bias and noise. However, it is expected that after improvements in UWB setup and calibration, the TraXYZ IMU also suffices. Besides the data quality, several research factors may cause limited performance. For example the method for determining initial orientation and the modelling of the UWB data. This will be discussed in the next section.

To conclude, when IMU data is incorporated into the TraXYZ system, a UWB/IMU EKF can be applied. This should be tuned so that a balance is found between smoothness and latency while keeping the values for noise covariance within a reasonable range. In general, tuning depends on how much trust is put in the IMU data relative to the UWB data. Accurate initial state estimation also increases performance. However, limitations of this algorithm were found that could not be resolved by tuning the algorithm. This research emphasized the importance of sufficiently accurate UWB data to maximize the algorithm's effectiveness. Hence it is recommended to look into UWB calibration. When data has improved, it is recommended to include IMU bias estimation, ZUPT, and NLOS detection into the EKF, as each of these methods showed their potential for improved tracking accuracy. Attaching multiple tags for coupled mutual position correction has benefits, as more clearly shown in the UWB/CVM case. One such is the reduced sensitivity to tuning variability. However, the technique studied in this thesis needs more research when IMU sensors are involved.

5-2 Future work

Following this research, it is recommended to start with obtaining a new dataset and repeat the research conducted in this report. Particularly, make sure the UWB setup has improved and the UWB system is well calibrated. The hypothesis is that this reduces most problems found in this research. Secondly, it might help to incorporate a different type of IMU sensor that contains less bias and noise. Once the research is tested with a better dataset, there are several additional suggestions to be considered. To start with, the UWB data can be modelled differently. For example, sometimes the data follows a heavy-tailed distribution due to outliers. The research in [9] discusses a method to implement this. Secondly, the UWB data can be preprocessed with a UWB/CVM EKF, creating a loosely coupled algorithm. This is similar to performing NLOS mitigation but based on the CVM instead of the IMU model. However, the purpose of incorporating an IMU sensor is then questioned. Concerning the IMU data, it is beneficial to analyze the bias by placing it stationary on a table and measuring from all six sides. This provides an indication of the bias, which can serve as an initial condition for bias estimation. In general, having a more accurate initial state is helpful. It is recommended to create a situation where the initial position of the artist in the UWB frame can be approximately determined. The artist should also begin in a way that allows their heading to be derived and then proceed to walk in that direction. Once the data quality is improved and the same sensors are used consistently, it is advised to thoroughly investigate the tuning parameters to ensure they can remain equal for different theatre productions. The values can also differ for Tag1 and Tag2. It can be allowed to let the values for noise covariance matrices vary per time step. Increasing the UWB measurement noise covariance over time may be beneficial for NLOS mitigation. Moreover, the NLOS mitigation can be performed by comparing the averaged position estimates of the two tags with the UWB distance measurements, provided the tags are joint. Regarding the UWB/IMU fusion with joint tags, it may be beneficial to perform the fixed distance update less frequently rather than at every timestep. Finally, if height estimation issues persist, a constant height update could be considered in the EKF.
Once the UWB/IMU fusion EKF has been thoroughly researched and possibly improved, related future research questions can be considered:

- Does this algorithm ensure that fewer UWB anchors are needed for accurate position estimation?
- How can the tags be weighed in the algorithm so that the most accurate tag is predominant in position estimation with joint tags?
- How can the height estimation be improved?
- Are there benefits to using a different fusing algorithm than the EKF?

Regarding research on tightly coupling two tags, the technique developed in this thesis was shown to work in the case of UWB/CVM. However, when orientation is involved by using IMU sensors, this technique needs more research. Potential solutions would be to further reduce IMU bias, or include a constant height update or constant inclination update in the EKF. Generally, it can be concluded that attaching multiple tags has benefits for position tracking accuracy. Averaging multiple loosely coupled tags already shows improvement. Tightly coupling the tags can provide additional benefits like corrected trajectories of the individual tags, preventing divergence due to strict NLOS mitigation, and reducing the algorithm's sensitivity to tuning variability. Therefore, fusing multiple tags shows potential for increased robustness against errors occurring in individual tags within general location tracking applications.

Appendix A

Jacobian matrices for UWB/IMU fusion EKF

A-1 Jacobian matrices for UWB/IMU fusion EKF

The EKF developed in Chapter 3 uses Jacobian matrices defined as $F_t^{(m)} = \frac{\partial f}{\partial x^{(m)}}\Big|_{x^{(m)}=\hat{x}_{t-1}^{(m)}}$ and $G_t^{(m)} = \frac{\partial f}{\partial e^{(m)}}\Big|_{x^{(m)}=\hat{x}_{t-1}^{(m)}}$, with f the dynamic IMU model of Eq. (2-4) and $x^{(m)} = (p,\ v,\ q)^\top$ the state of tag $m \in \{1, 2\}$. This results in the expressions for $F_t^{(m)}$ and $G_t^{(m)}$ for each tag $m \in \{1, 2\}$

$$F_t^{(m)} = \begin{bmatrix} I_{3\times3} & \Delta t \cdot I_{3\times3} & \frac{(\Delta t)^2}{2}\left[\frac{\partial R^{nb}}{\partial q_0},\ \frac{\partial R^{nb}}{\partial q_1},\ \frac{\partial R^{nb}}{\partial q_2},\ \frac{\partial R^{nb}}{\partial q_3}\right]\Big|_{q=\hat{q}_{t-1}^{(m)}} \cdot y_{a,t}^{(m)} \\ 0 & I_{3\times3} & \Delta t\left[\frac{\partial R^{nb}}{\partial q_0},\ \frac{\partial R^{nb}}{\partial q_1},\ \frac{\partial R^{nb}}{\partial q_2},\ \frac{\partial R^{nb}}{\partial q_3}\right]\Big|_{q=\hat{q}_{t-1}^{(m)}} \cdot y_{a,t}^{(m)} \\ 0 & 0 & I_{4\times4} + \frac{\Delta t}{2} S(y_{\omega,t}^{(m)}) \end{bmatrix} \in \mathbb{R}^{10\times10}, \quad \text{(A-1)}$$

$$G_t^{(m)} = \begin{bmatrix} \frac{(\Delta t)^2}{2} \cdot I_{3\times3} & 0 & 0 \\ 0 & \Delta t \cdot I_{3\times3} & 0 \\ 0 & 0 & \frac{\Delta t}{2}\bar{S}(\hat{q}_{t-1}^{(m)}) \end{bmatrix} \in \mathbb{R}^{10\times9}, \quad \text{(A-2)}$$

with Δt the time difference between consecutive measurements provided by tag m specifically, R^{nb} given in Eq. (2-5), and S and $\bar{S}$ are given in Eq. (2-6) and Eq. (2-7), respectively. Note that in the calculation of $G_t^{(m)}$, the negative sign of $e_{a,t}$ and the multiplication of R_t^{nb} with $e_{a,t}$ in the model of Eq. (2-4) are omitted without loss of generality [13].

The Jacobian matrix in the EKF measurement update is defined as $H_t^{i,\text{UWB}} = \frac{\partial h_i}{\partial x^{(m)}}\Big|_{x^{(m)}=\hat{x}_t^{(m)}}$ for each UWB ranging measurement i at time t, where $y_{d,t}^i = h_i(x, p_{\text{anc}}^i) + e_{d,t}^i$ is the measurement model in Eq. (2-1). Hence $h_i(x, p_{\text{anc}}^i) = \|p_{\text{anc}}^i - p_t\|_2$. The expression for $H_t^{(m),\text{UWB}}$ for

the measurements i provided by tag $m \in \{1, 2\}$ is then

$$H_t^{(m),\text{UWB}} = \begin{bmatrix} \frac{-(p^1_{\text{anc},x} - \hat{p}^{(m)}_{x,t})}{\|p^1_{\text{anc}} - \hat{p}^{(m)}_t\|_2} & \frac{-(p^1_{\text{anc},y} - \hat{p}^{(m)}_{y,t})}{\|p^1_{\text{anc}} - \hat{p}^{(m)}_t\|_2} & \frac{-(p^1_{\text{anc},z} - \hat{p}^{(m)}_{z,t})}{\|p^1_{\text{anc}} - \hat{p}^{(m)}_t\|_2} & 0 & \dots & 0 \\ & \vdots & & & & \\ \frac{-(p^i_{\text{anc},x} - \hat{p}^{(m)}_{x,t})}{\|p^i_{\text{anc}} - \hat{p}^{(m)}_t\|_2} & \frac{-(p^i_{\text{anc},y} - \hat{p}^{(m)}_{y,t})}{\|p^i_{\text{anc}} - \hat{p}^{(m)}_t\|_2} & \frac{-(p^i_{\text{anc},z} - \hat{p}^{(m)}_{z,t})}{\|p^i_{\text{anc}} - \hat{p}^{(m)}_t\|_2} & 0 & \dots & 0 \end{bmatrix} \in \mathbb{R}^{\#y^{(m)}_{d,t} \times 10}, \quad \text{(A-3)}$$

where $y^{(m)}_{d,t}$ contains all UWB measurements i provided by tag $m \in \{1, 2\}$ and $\hat{p}^{(m)}_{x,t}$, $\hat{p}^{(m)}_{y,t}$, $\hat{p}^{(m)}_{z,t}$ represent the x, y and z coordinate of the position $\hat{p}^{(m)}_t$.

A-2 Jacobian matrices for UWB/IMU fusion EKF with bias estimation

If the bias is estimated in the state of the EKF, the state is augmented to $x_t = (p^n_t,\ v^n_t,\ q^{nb}_t,\ \delta^b_{a,t},\ \delta^b_{\omega,t})^\top$ and the model f is augmented with the random walks in Eq. (3-9), then $F^{(m)}_t$ and $G^{(m)}_t$ are adjusted to

$$F^{(m)}_t = \begin{bmatrix} I_{3\times3} & \Delta t \cdot I_{3\times3} & \frac{(\Delta t)^2}{2}\left[\frac{\partial R^{nb}}{\partial q_0},\ \frac{\partial R^{nb}}{\partial q_1},\ \frac{\partial R^{nb}}{\partial q_2},\ \frac{\partial R^{nb}}{\partial q_3}\right]\Big|_{q=\hat{q}^{(m)}_{t-1}} \cdot (y^{(m)}_{a,t} - \hat{\delta}^{(m)}_{a,t-1}) & -\frac{(\Delta t)^2}{2} R^{nb}\Big|_{q=\hat{q}^{(m)}_{t-1}} & 0 \\ 0 & I_{3\times3} & \Delta t\left[\frac{\partial R^{nb}}{\partial q_0},\ \frac{\partial R^{nb}}{\partial q_1},\ \frac{\partial R^{nb}}{\partial q_2},\ \frac{\partial R^{nb}}{\partial q_3}\right]\Big|_{q=\hat{q}^{(m)}_{t-1}} \cdot (y^{(m)}_{a,t} - \hat{\delta}^{(m)}_{a,t-1}) & -\frac{(\Delta t)^2}{2} R^{nb}\Big|_{q=\hat{q}^{(m)}_{t-1}} & 0 \\ 0 & 0 & I_{4\times4} + \frac{\Delta t}{2} S(y^{(m)}_{\omega,t} - \hat{\delta}^{(m)}_{\omega,t-1}) & 0 & \frac{\Delta t}{2}\frac{\partial S(y^{(m)}_{\omega,t} - \delta_{\omega,t})}{\partial \delta_{\omega,t}} \cdot \hat{q}^{(m)}_{t-1} \\ 0 & 0 & 0 & I_{3\times3} & 0 \\ 0 & 0 & 0 & 0 & I_{3\times3} \end{bmatrix} \in \mathbb{R}^{16\times16}, \quad \text{(A-4)}$$

with Δt the time difference between consecutive measurements provided by tag m specifically, R^{nb} given in Eq. (2-5), and S given in Eq. (2-6). Furthermore,

$$\frac{\Delta t}{2}\frac{\partial S(y^{(m)}_{\omega,t} - \delta_{\omega,t})}{\partial \delta_{\omega,t}} \cdot \hat{q}^{(m)}_{t-1} = \frac{\Delta t}{2}\begin{bmatrix} \hat{q}^{(m)}_1 & \hat{q}^{(m)}_2 & \hat{q}^{(m)}_3 \\ -\hat{q}^{(m)}_0 & \hat{q}^{(m)}_3 & -\hat{q}^{(m)}_2 \\ -\hat{q}^{(m)}_3 & -\hat{q}^{(m)}_0 & \hat{q}^{(m)}_1 \\ \hat{q}^{(m)}_2 & -\hat{q}^{(m)}_1 & -\hat{q}^{(m)}_0 \end{bmatrix}. \quad \text{(A-5)}$$

$$G^{(m)}_t = \begin{bmatrix} \frac{(\Delta t)^2}{2} \cdot I_{3\times3} & 0 & 0 & 0 & 0 \\ 0 & \Delta t \cdot I_{3\times3} & 0 & 0 & 0 \\ 0 & 0 & \frac{\Delta t}{2}\bar{S}(\hat{q}^{(m)}_{t-1}) & 0 & 0 \\ 0 & 0 & 0 & I_{3\times3} & 0 \\ 0 & 0 & 0 & 0 & I_{3\times3} \end{bmatrix} \in \mathbb{R}^{16\times15}, \quad \text{(A-6)}$$

with $\bar{S}$ given in Eq. (2-7).

A-3 Jacobian matrix for UWB/IMU fusion EKF with tightly coupled tags

To fuse the data of the two tags in an EKF, the EKF measurement update is augmented with an equality constraint on the relative distance between the tags. The equations use the Jacobian of $\|Lx\|_2$ evaluated at $x = \hat{x}$. The expression for the Jacobian H_t^L is

$$H_t^L = \begin{bmatrix} \frac{\hat{p}_{x,t}^{(1)} - \hat{p}_{x,t}^{(2)}}{\|\hat{p}_t^{(1)} - \hat{p}_t^{(2)}\|_2} & \frac{\hat{p}_{y,t}^{(1)} - \hat{p}_{y,t}^{(2)}}{\|\hat{p}_t^{(1)} - \hat{p}_t^{(2)}\|_2} & \frac{\hat{p}_{z,t}^{(1)} - \hat{p}_{z,t}^{(2)}}{\|\hat{p}_t^{(1)} - \hat{p}_t^{(2)}\|_2} & 0 & \cdots \\ \cdots & 0 & \frac{\hat{p}_{x,t}^{(1)} - \hat{p}_{x,t}^{(2)}}{\|\hat{p}_t^{(1)} - \hat{p}_t^{(2)}\|_2} & \frac{\hat{p}_{y,t}^{(1)} - \hat{p}_{y,t}^{(2)}}{\|\hat{p}_t^{(1)} - \hat{p}_t^{(2)}\|_2} & \frac{\hat{p}_{z,t}^{(1)} - \hat{p}_{z,t}^{(2)}}{\|\hat{p}_t^{(1)} - \hat{p}_t^{(2)}\|_2} & 0 & \cdots & 0 \end{bmatrix} \in \mathbb{R}^{1 \times (n_1 + n_2)}, \tag{A-7}$$

with n_1, n_2 the number of states of Tag1 and Tag2, respectively, and $\hat{p}_{x,t}^{(m)}$, $\hat{p}_{y,t}^{(m)}$, $\hat{p}_{z,t}^{(m)}$ represent the x, y and z coordinate of the position $\hat{p}_t^{(m)}$ for tag $m \in \{1, 2\}$.

Appendix B

Additional results

B-1 Bias estimation results

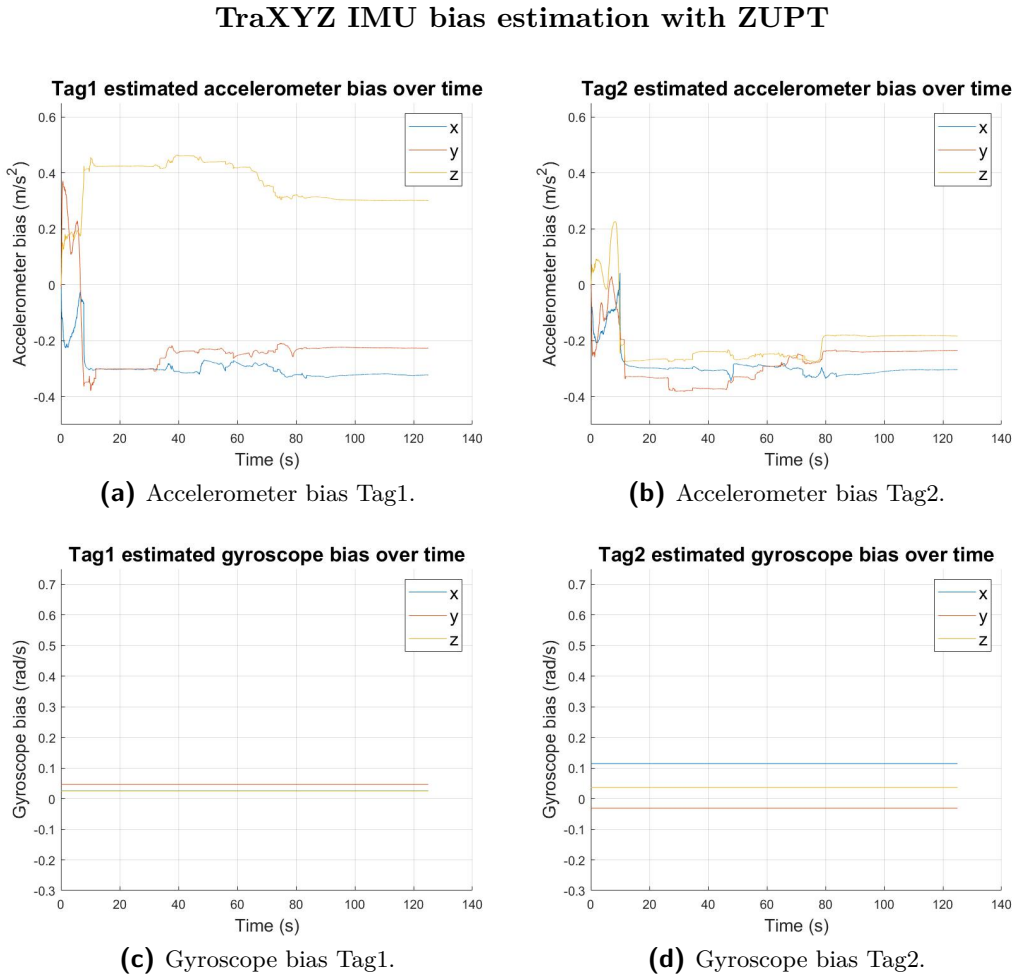

(a) Accelerometer bias Tag1.

(b) Accelerometer bias Tag2.

(c) Gyroscope bias Tag1.

(d) Gyroscope bias Tag2.

Figure B-1: Estimated IMU bias over time when only accelerometer bias is estimated and gyroscope bias is fixed over time. Additionally a ZUPT is applied.

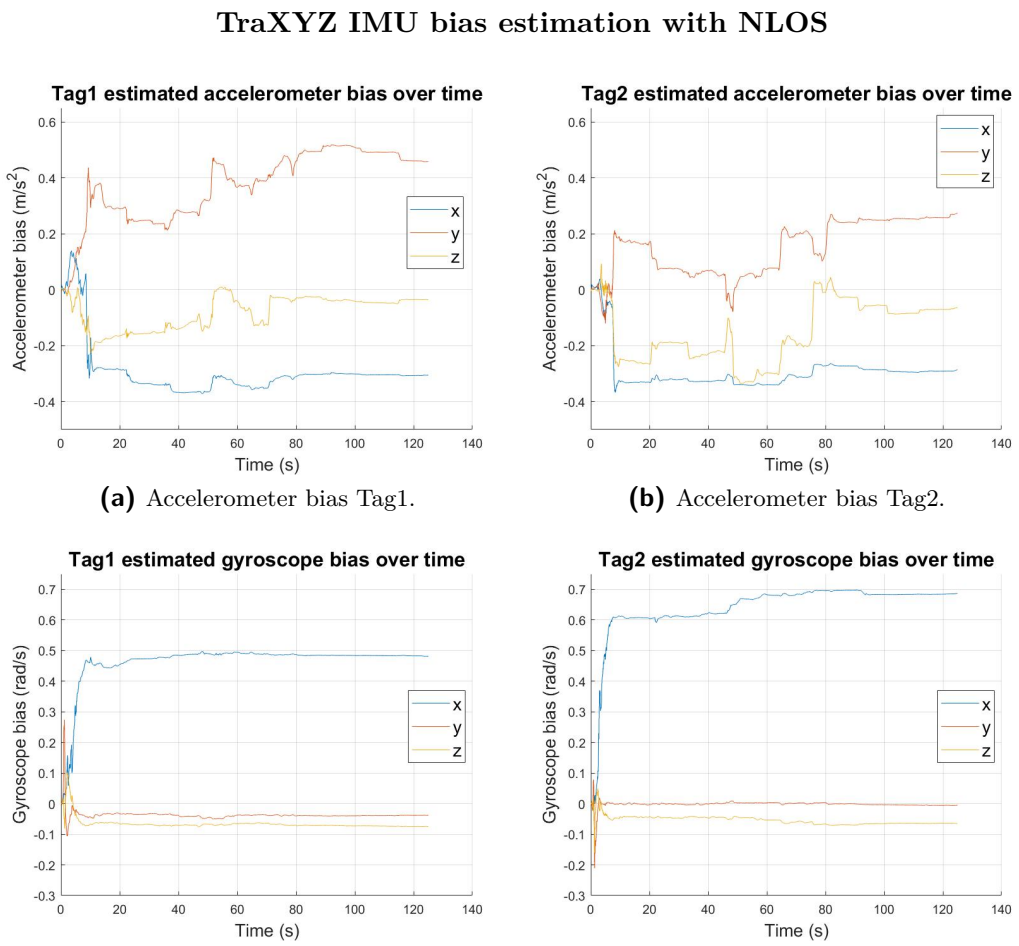

(a) Accelerometer bias Tag1.

(b) Accelerometer bias Tag2.

(c) Gyroscope bias Tag1.

(d) Gyroscope bias Tag2.

Figure B-2: Estimated IMU bias over time when additionally NLOS mitigation is applied.

B-2 UWB/IMU EKF joint tags results

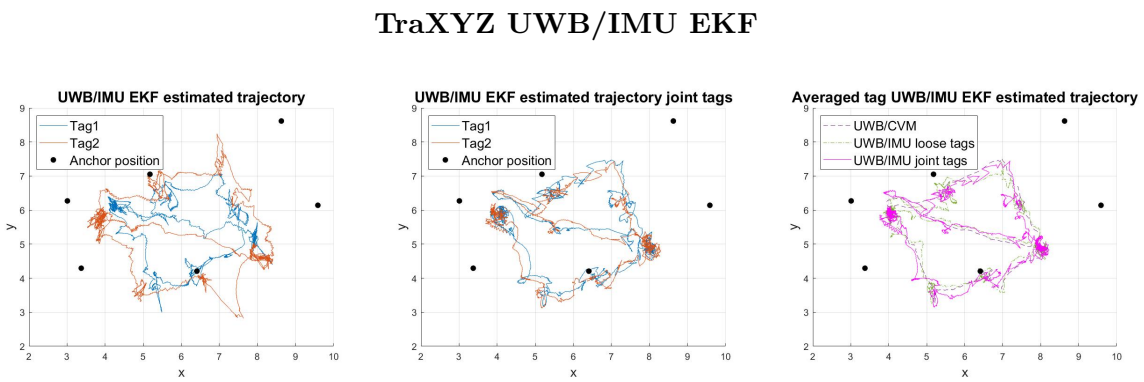

(a) Trajectory Tag1 and Tag2, loose tags.

(b) Trajectory Tag1 and Tag2, joint tags.

(c) Trajectory averaged tags.

Figure B-3: Position coordinates estimated with UWB measurements and an EKF with an IMU model in the time update, for loose tags and joint tags. In the joint tag update the noise covariance is set to $R_t^L = 10^{-6}$. No bias correction, ZUPT, or NLOS mitigation is applied.

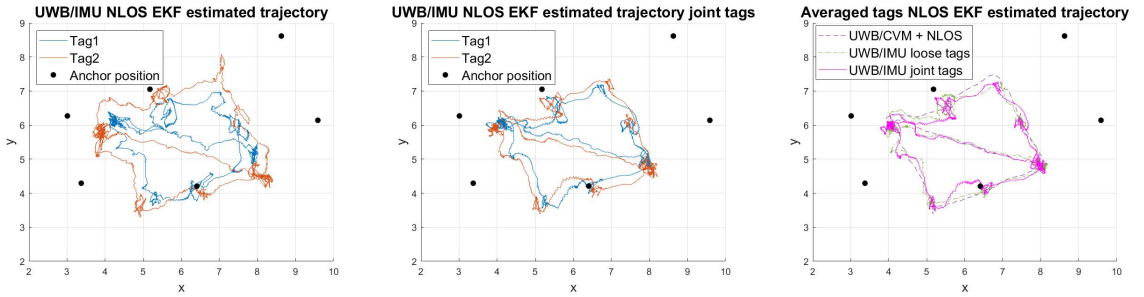

(a) Trajectory Tag1 and Tag2, loose tags.

(b) Trajectory Tag1 and Tag2, joint tags.

(c) Trajectory averaged tags.

Figure B-4: Position coordinates estimated with UWB measurements and an EKF with an IMU model in the time update, for loose tags and joint tags. NLOS mitigation is applied where $R_t^{\text{UWB}} = 0.4$ to calculate the confidence interval and $R_t^{\text{UWB}} = 0.25$ for the remaining UWB measurements. No bias correction or ZUPT is applied.

TraXYZ UWB/IMU EKF + ZUPT

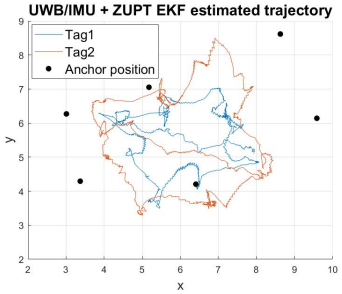

(a) Trajectory Tag1 and Tag2, loose tags.

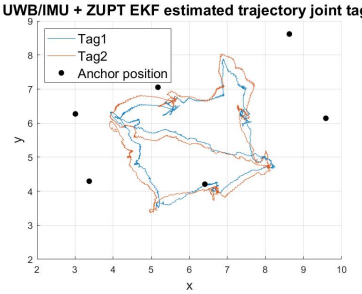

(b) Trajectory Tag1 and Tag2, joint tags.

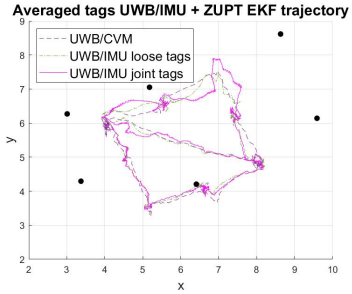

(c) Trajectory averaged tags.

Figure B-5: Position coordinates estimated with UWB measurements and an EKF with an IMU model in the time update, for loose tags and joint tags. A ZUPT is applied. No bias correction or NLOS mitigation is applied.

TraXYZ UWB/IMU EKF + accelerometer bias estimation + ZUPT

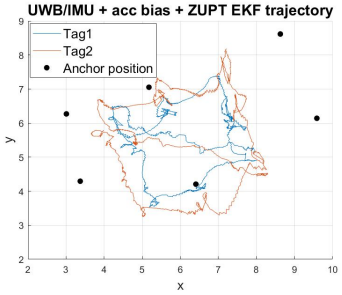

(a) Trajectory Tag1 and Tag2, loose tags.

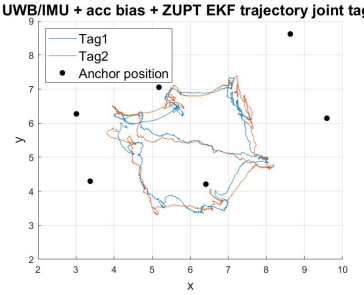

(b) Trajectory Tag1 and Tag2, joint tags.

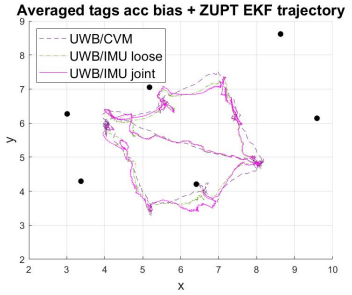

(c) Trajectory averaged tags.

Figure B-6: Position coordinates estimated with UWB measurements and an EKF with an IMU model in the time update, for loose tags and joint tags. A ZUPT is applied. Only accelerometer bias is estimated. Gyroscope bias is fixed. No NLOS mitigation is applied.

Bibliography

[1] Sendrato, "In the spotlight." https://www.traxyz.com/, 2024. [Online]. Accessed: Oct. 14, 2024.

[2] F. Zafari, A. Gkelias, and K. K. Leung, "A survey of indoor localization systems and technologies," *IEEE Communications Surveys Tutorials*, vol. 21, no. 3, pp. 2568–2599, 2019.

[3] H. Zhang, Z. Zhang, R. Zhao, J. Lu, Y. Wang, and P. Jia, "Review on UWB-based and multi-sensor fusion positioning algorithms in indoor environment," in *2021 IEEE 5th Advanced Information Technology, Electronic and Automation Control Conference (IAEAC)*, vol. 5, pp. 1594–1598, 2021.

[4] H. Obeidat, W. Shuaieb, O. Obeidat, and R. Abd-Alhameed, "A review of indoor localization techniques and wireless technologies," *Wireless Personal Communications*, vol. 119, no. 1, p. 289–327, 2021.

[5] S. Sharma Sivadevuni and S. K. Ravichandran, "Tracking and localization of devices - an IoT review," in *2023 International Conference on Inventive Computation Technologies (ICICT)*, pp. 1321–1325, 2023.

[6] A. K. Paul and T. Sato, "Localization in wireless sensor networks: A survey on algorithms, measurement techniques, applications and challenges," *Journal of Sensor and Actuator Networks*, vol. 6, no. 4, 2017.

[7] S. Kumar and R. M. Hegde, "A review of localization and tracking algorithms in wireless sensor networks," 2017.

[8] C. Liu, T. Kadja, and V. P. Chodavarapu, "Experimental evaluation of sensor fusion of low-cost UWB and IMU for localization under indoor dynamic testing conditions," *Sensors*, vol. 22, no. 21, 2022.

[9] M. Kok, J. D. Hol, and T. B. Schön, "Indoor positioning using ultrawideband and inertial measurements," *IEEE Transactions on Vehicular Technology*, vol. 64, no. 4, pp. 1293–1303, 2015.

[10] T. Laadung, S. Ulp, A. Fjodorov, M. M. Alam, and Y. Le Moullec, "Adaptive extended kalman filter position estimation based on ultra-wideband active-passive ranging protocol," *IEEE Access*, vol. 11, pp. 92575–92588, 2023.

[11] N. Borhan, I. Saleh, A. Yunus, W. Rahiman, D. Novaliendry, and Risfendra, "Reducing UWB indoor localization error using the fusion of kalman filter with moving average filter," in *2023 IEEE International Conference on Automatic Control and Intelligent Systems (I2CACIS)*, pp. 55–59, 2023.

[12] A. Zou, W. Hu, Y. Luo, and P. Jiang, "An improved UWB/IMU tightly coupled positioning algorithm study," *Sensors*, vol. 23, no. 13, 2023.

[13] M. Kok, J. D. Hol, and T. B. Schön, "Using inertial sensors for position and orientation estimation," *Foundations and Trends in Signal Processing*, vol. 11, no. 1-2, pp. 1–153, 2017.

[14] S. Djosic, I. Stojanovic, M. Jovanovic, and G. L. Djordjevic, "Multi-algorithm UWB-based localization method for mixed LOS/NLOS environments," *Computer Communications*, vol. 181, pp. 365–373, 2022.

[15] I. Skog, J.-O. Nilsson, D. Zachariah, and P. Händel, "Fusing the information from two navigation systems using an upper bound on their maximum spatial separation," in *2012 International Conference on Indoor Positioning and Indoor Navigation (IPIN)*, pp. 1–5, 2012.

[16] F. Gustafsson, *Statistical sensor fusion.* Studentlitteratur, 2 ed., 2012.

[17] J. D. Hol, *Sensor fusion and calibration of inertial sensors, vision, ultra-wideband and GPS.* Ph.D. dissertation, Linköping University, Sweden, 2011.

[18] F. Hölzke, H. Borstell, F. Golatowski, and C. Haubelt, "Pedestrian localization with stride-wise error estimation and compensation by fusion of UWB and IMU data," *Sensors*, vol. 23, no. 10, 2023.

[19] S. Zihajehzadeh, P. K. Yoon, and E. J. Park, "A magnetometer-free indoor human localization based on loosely coupled IMU/UWB fusion," in *2015 37th Annual International Conference of the IEEE Engineering in Medicine and Biology Society (EMBC)*, pp. 3141–3144, 2015.

[20] L. Zwirello, X. Li, T. Zwick, C. Ascher, S. Werling, and G. F. Trommer, "Sensor data fusion in UWB-supported inertial navigation systems for indoor navigation," in *2013 IEEE International Conference on Robotics and Automation*, pp. 3154–3159, 2013.

[21] S. Zheng, Z. Li, Y. Liu, H. Zhang, and X. Zou, "An optimization-based UWB-IMU fusion framework for UGV," *IEEE Sensors Journal*, vol. 22, no. 5, pp. 4369–4377, 2022.

[22] S. Jang, B. An, S. Yoon, and K. Lim, "Research on the indoor environment positioning algorithm using sensor fusion," in *2023 International Conference on Electronics, Information, and Communication (ICEIC)*, pp. 1–4, 2023.

[23] J. D. Hol, F. Dijkstra, H. Luinge, and T. B. Schön, "Tightly coupled UWB/IMU pose estimation," pp. 688 – 692, October 2009.

[24] Y. Xu, Y. Shmaliy, C. K. Ahn, G. Tian, and X. Chen, "Robust and accurate UWB-based indoor robot localisation using integrated EKF/EFIR filtering," *IET Radar, Sonar Navigation*, vol. 12, 03 2018.

[25] M. Granados-Cruz, Y. Shmaliy, O. Ibarra-Manzano, S. Zhao, and S. Khan, "Iterative algorithms for extended unbiased FIR filtering of nonlinear models over sensor networks," 12 2015.

[26] M. Granados-Cruz, Y. S. Shmaliy, and S. Zhao, "A generalized algorithm for nonlinear state estimation using extended UFIR filtering," pp. 1–6, 2014.

[27] X. Yang, J. Wang, D. Song, B. Feng, and H. Ye, "A novel NLOS error compensation method based IMU for UWB indoor positioning system," *IEEE Sensors Journal*, vol. 21, no. 9, pp. 11203–11212, 2021.

[28] M. R. Gholami, E. G. Ström, F. Sottile, D. Dardari, A. Conti, S. Gezici, M. Rydström, and M. A. Spirito, "Static positioning using UWB range measurements," in *2010 Future Network Mobile Summit*, pp. 1–10, 2010.

[29] J. M. Pak, P. S. Kim, S. H. You, S. S. Lee, and M. K. Song, "Extended least square unbiased FIR filter for target tracking using the constant velocity motion model," *International Journal of Control, Automation and Systems*, vol. 15, pp. 947–951, April 2017.

[30] S. Särkkä, *Bayesian Filtering and Smoothing*. Cambridge University Press, 2 ed., 2023.

[31] R. Ali, R. Liu, A. Nayyar, B. Qureshi, and Z. Cao, "Tightly coupling fusion of UWB ranging and IMU pedestrian dead reckoning for indoor localization," *IEEE Access*, vol. 9, pp. 164206–164222, 2021.

[32] I. Ullah, Y. Shen, X. Su, C. Esposito, and C. Choi, "A localization based on unscented kalman filter and particle filter localization algorithms," *IEEE Access*, vol. 8, pp. 2233–2246, 2020.

[33] W. Guosheng, Q. Shuqi, L. Qiang, W. Heng, L. Huican, and L. Bing, "UWB and IMU system fusion for indoor navigation," in *2018 37th Chinese Control Conference (CCC)*, pp. 4946–4950, 2018.

[34] Z. Zeng, S. Liu, and L. Wang, "A novel NLOS mitigation approach for TDOA based on IMU measurements," in *2018 IEEE Wireless Communications and Networking Conference (WCNC)*, pp. 1–6, 2018.

[35] A. M. M. Almassri, N. Shirasawa, A. Purev, K. Uehara, W. Oshiumi, S. Mishima, and H. Wagatsuma, "Artificial neural network approach to guarantee the positioning accuracy of moving robots by using the integration of IMU/UWB with motion capture system data fusion," *Sensors*, vol. 22, no. 15, 2022.

[36] R. Vleugels, B. Van Herbruggen, J. Fontaine, and E. De Poorter, "Ultra-wideband indoor positioning and IMU-based activity recognition for ice hockey analytics," *Sensors*, vol. 21, no. 14, 2021.

[37] W. You, F. Li, L. Liao, and M. Huang, "Data fusion of UWB and IMU based on unscented kalman filter for indoor localization of quadrotor UAV," *IEEE Access*, vol. 8, pp. 64971–64981, 2020.

[38] H. A. Hashim, A. E. E. Eltoukhy, and K. G. Vamvoudakis, "UWB ranging and IMU data fusion: Overview and nonlinear stochastic filter for inertial navigation," *IEEE Transactions on Intelligent Transportation Systems*, pp. 1–0, 2023.

[39] D. Feng, C. Wang, C. He, Y. Zhuang, and X.-G. Xia, "Kalman-filter-based integration of IMU and UWB for high-accuracy indoor positioning and navigation," *IEEE Internet of Things Journal*, vol. 7, no. 4, pp. 3133–3146, 2020.

[40] Y. Wang and X. Li, "Graph-optimization-based ZUPT/UWB fusion algorithm," *ISPRS International Journal of Geo-Information*, vol. 7, no. 1, 2018.

[41] G. Prateek, R. Girisha, K. Hari, and P. Händel, "Data fusion of dual foot-mounted INS to reduce the systematic heading drift," in *2013 4th International Conference on Intelligent Systems, Modelling and Simulation*, pp. 208–213, 2013.

[42] X. Ma and S. Särkkä, "Indoor positioning methods based on dual feet-mounted IMUs with distance constraints," in *2023 13th International Conference on Indoor Positioning and Indoor Navigation (IPIN)*, 2023.

[43] D. Simon, "Kalman filtering with state constraints: A survey of linear and nonlinear algorithms," *Control Theory Applications, IET*, vol. 4, pp. 1303 – 1318, 09 2010.

[44] Q. Zeng, Y. Jin, H. Yu, and X. You, "A UAV localization system based on double UWB tags and IMU for landing platform," *IEEE Sensors Journal*, vol. 23, no. 9, pp. 10100–10108, 2023.

[45] D. Simón Colomar, J.-O. Nilsson, and P. Händel, "Smoothing for ZUPT-aided INSs," in *2012 International Conference on Indoor Positioning and Indoor Navigation (IPIN)*, pp. 1–5, 2012.

[46] A. Shakerian, A. Eghmazi, J. Goasdoué, and R. J. Landry, "A secure ZUPT-aided indoor navigation system using blockchain in GNSS-denied environments," *Sensors*, vol. 23, no. 14, 2023.

[47] I. Skog, J.-O. Nilsson, and P. Händel, "Evaluation of zero-velocity detectors for foot-mounted inertial navigation systems," in *2010 International Conference on Indoor Positioning and Indoor Navigation*, pp. 1–6, 2010.

[48] J. Li, Y. Wang, Z. Chen, L. Ma, and S. Yan, "Improved height estimation using extended kalman filter on uwb-barometer 3d indoor positioning system," *Wireless Communications and Mobile Computing*, vol. 2021, no. 1, p. 7057513, 2021.

[49] X. Ma and S. Särkkä, "Spacing vector and varying distance constrained positioning using dual feet-mounted imus," *IEEE Transactions on Instrumentation and Measurement*, vol. 73, pp. 1–11, 2024.

[50] J. Wahlström and I. Skog, "Fifteen years of progress at zero velocity: A review," *IEEE Sensors Journal*, vol. 21, no. 2, pp. 1139–1151, 2021.

[51] J.-O. Nilsson, I. Skog, and P. Handel, "A note on the limitations of zupts and the implications on sensor error modeling," p. 4, 2012.

[52] A. Jiménez, F. Seco, J. Prieto, and J. Guevara, "Indoor pedestrian navigation using an ins/ekf framework for yaw drift reduction and a foot-mounted imu," in *2010 7th Workshop on Positioning, Navigation and Communication*, pp. 135–143, 2010.

Glossary

List of Acronyms

CVM	Constant Velocity Model
EFIR	Extended Finite Impulse Response
EKF	Extended Kalman Filter
GPS	Global Positioning System
IMU	Inertial Measurement Unit
KF	Kalman Filter
LiDAR	Light Detection And Ranging
NLOS	Non-Line-of-Sight
NLS	Non-Linear Least Squares
PF	Particle Filter
SHOD	Stance Hypothesis Optimal Detector
ToF	Time of Flight
TWR	Two Way Ranging
UKF	Unscented Kalman Filter
UWB	Ultra-Wideband
ZUPT	Zero Velocity Update